Technical Report Documentation Page

1. Report No MPM-10	2. Government Accession No.	3. Recipient's Catalog No.
4. Title and Subtitle **Effects of Aggregate Angularity on Mix Design Characteristics and Pavement Performance**		5. Report Date December 02, 2009
		6. Performing Organization Code
7. Author/s **Leonardo, T. Souza and Yongrak Kim**		8. Performing Organization Report No. MPM-10
9. Performing Organization Name and Address University of Nebraska-Lincoln (Department of Civil Engineering) W351 NH, PO Box 880531, Lincoln, NE 68588		10. Work Unit No. (TRAIS)
		11. Contract or Grant No. 26-1107-0107-001
12. Sponsoring Organization Name and Address Nebraska Department of Roads (NDOR) 1400 Highway 2, PO Box 94759, Lincoln, NE 68509		13. Type of Report and Period Covered
		14. Sponsoring Agency Code
15. Supplementary Notes		

16. Abstract

This research targets two primary purposes: to estimate current aggregate angularity test methods and to evaluate current aggregate angularity requirements in the Nebraska asphalt mixture/pavement specification. To meet the first research objective, various aggregate angularity tests are estimated with the same sets of aggregates and are compared by investigating their characteristics on testing repeatability, cost, testing time, workability, and sensitivity of test results. For the second objective, the effect of aggregate angularity on mixture performance is investigated by conducting laboratory performance tests (the uniaxial static creep test and the indirect tensile fracture energy test) of five mixes designed with different combinations of coarse and fine aggregate angularity and statistical analyses of five-year asphalt pavement analyzer test results of field mixtures. Results from the indirect tensile fracture energy test are then incorporated with finite element simulations of virtual specimens, which attempt to explore the detailed mechanisms of cracking related to the aggregate angularity. Results from the estimation of various angularity test methods imply that for the coarse aggregate angularity measurement, the AASHTO T326 method looks better than the current Superpave method, ASTM D5821, in that it is more objective and is very simple to perform with much less testing time. For the fine aggregate angularity measurement, the current Superpave testing method, AASHTO T304, is considered reasonable in a practical sense. Rutting performance test results indicate that higher angularity in the mixture improves rut resistance due to better aggregate interlocking. The overall effect of angularity on the mixtures' resistance to fatigue damage is positive because aggregate blends with higher angularity require more binder to meet mix design criteria, which mitigates cracking due to increased viscoelastic energy dissipation from the binder, while angular particles produce a higher stress concentration that results in potential cracks. Finite element simulations of virtual specimens support findings from experimental tests. Outcomes from this research are expected to potentially improve current Nebraska asphalt specifications, particularly for aggregate angularity requirements and test methods to characterize local aggregate angularity.

17. Key Words Aggregate Angularity, Asphalt Mixture, Pavement, Performance, Finite Element Modeling	18. Distribution Statement		
19. Security Classification (of this report) Unclassified	20. Security Classification (of this page) Unclassified	21. No. of Pages 88	22. Price

Form DOT F 1700.7 (8-72) Reproduction of form and completed page is authorized

DISCLAIMER

This report was funded in part through grant[s] from the Federal Highway Administration [and Federal Transit Administration], U.S. Department of Transportation. The views and opinions of the authors [or agency] expressed herein do not necessarily state or reflect those of the U. S. Department of Transportation.

TABLE OF CONTENTS

CHAPTER		Page
I	INTRODUCTION	7
	Research Objectives	9
	Research Scope	9
	Organization of the Report	10
II	BACKGROUND	11
	Test Methods to Estimate Aggregate Angularity	13
	Effect of Aggregate Angularity on HMA Performance	19
III	RESEARCH METHODOLOGY	26
	Materials Selection	26
	Mix Design Method	29
	Aggregate Angularity Tests Performed	32
	Performance Tests of Mixtures	43
	Finite Element Modeling of IDT Fracture Testing	52
IV	RESULTS AND DISCUSSION	59
	Mix Design Results	59
	Laboratory Performance Test Results	60
	Finite Element Model Simulation Results	65
	Angularity Test Results and Discussion	70
V	SUMMARY AND CONCLUSIONS	77
	Conclusions	77
	NDOR Implementation Plan	79
REFERENCES		80
ACKNOWLEDGMENTS		88

LIST OF FIGURES

FIGURE		Page
2.1.	Aggregate Shape Characteristics (Sukhwani et al. 2006)	11
3.1.	A Target Gradation Curve of Aggregate Blends	30
3.2.	Gradation Curves of the Asphalt Mixtures and the FAM Mixtures	31
3.3.	Internal Microstructure of (a) FAM Mixture; (b) Asphalt Concrete Mixture	32
3.4.	Definition of Fractured Face (ASTM D5821)	33
3.5.	Aggregates with Different Angularity Characteristics	34
3.6.	Correlation between Aggregate Angularity and Voids	35
3.7.	Apparatus of the AASHTO T326 Test	35
3.8.	AIMS Device	36
3.9.	AIMS Interface for Coarse Aggregates	37
3.10.	AIMS Gradient Method to Quantify Angularity	38
3.11.	Steps of the Two-Dimensional Digital Image Processing	39
3.12.	AASHTO T304 Testing Apparatus	41
3.13.	AIMS Interface for Fine Aggregates	43
3.14.	A Specimen Cored and Sawed from the Gyratory Compacted Sample	44
3.15.	A Device Used to Place the Mounting Studs for LVDTs	44
3.16.	A Specimen with LVDTs Mounted in the UTM-25kN	45
3.17.	Typical Test Results of the Uniaxial Static Creep Test	46
3.18.	Asphalt Pavement Analyzer (APA)	47
3.19.	Relationship between Field Fatigue Performance and IDT Fracture Energy (Kim et al. 2002)	48

FIGURE Page

3.20. Testing Specimens after Coring-Sawing Process 49

3.21. Gauge-Point Mounting Device 49

3.22. An IDT Specimen Installed in the UTM-25kN 50

3.23. Typical Stress-Strain Plot of the IDT Fracture Test 52

3.24. Several Internal Microstructures Virtually Generated 54

3.25. Finite Element Mesh of the Virtual Specimen 55

3.26. Schematic Representation of the Cohesive Zone Concept 57

4.1. Uniaxial Static Creep Test Results 60

4.2. APA Test Results of *SP2* Mixtures 61

4.3. APA Test Results of *SP4* Mixtures 62

4.4. APA Test Results of *SP4S* Mixtures 62

4.5. APA Test Results of *SP5* Mixtures 63

4.6. IDT Fracture Energy Test Results from Asphalt Concrete Specimens ... 64

4.7. IDT Fracture Energy Test Results from Fine Aggregate Matrix Specimens 65

4.8. Virtual IDT Specimens Produced for the FE Simulations 66

4.9. Finite Element Simulation Results of the IDT Fracture Energy Test 68

4.10. Deformation and Crack Growth of the Specimen (Shown in Figure 4.8(b)) at Two Different Loading Stages (at the Peak Force and Near Failure).. 69

4.11. Comparison of Elemental Stress Contour Plots 70

LIST OF TABLES

TABLE		Page
2.1.	Advantages and Disadvantages of the Testing Methods Used to Measure Aggregate Characteristics (reproduced from Masad et al. 2007)	16
2.2.	Features of Test Methods for Experimental Evaluation (reproduced from Masad et al. 2007)……..……...	18
3.1.	Fundamental Properties of Aggregates	27
3.2.	Asphalt Binder Properties of PG 64-28	28
3.3.	Physical Properties of Hydrated Lime	28
3.4.	Chemical Properties of Hydrated Lime	29
3.5.	Five Mixtures Designed for This Study	30
3.6.	Sample Size of AIMS for Fine Aggregates	42
3.7.	Parameters in Equation [3.5]	51
4.1.	Volumetric Mix Properties	59
4.2.	Linear Elastic and Linear Viscoelastic Material Properties	66
4.3.	Cohesive Zone Properties Assumed for This Study	67
4.4.	Summary of Coarse Aggregate Angularity Tests	71
4.5.	Summary of Fine Aggregate Angularity Tests	72
4.6.	Repeatability Analysis Results	73
4.7.	Estimated Price of Each Test Method	73
4.8.	Testing Time Spent to Perform Each Angularity Test	74
4.9.	Testing Sensitivity of Each Angularity Test	75
4.10.	Ranking of Coarse Aggregate Angularity Tests for Each Category	76
4.11.	Ranking of Fine Aggregate Angularity Tests for Each Category	76

CHAPTER 1
INTRODUCTION

Since aggregates make up between 80% and 90% of the total volume or 94% to 95% of the mass of hot-mix asphalt (HMA), the quality of the aggregate significantly influences pavement performance. Aggregate geometry consists of three independent characteristics, form, angularity (or roundness), and surface texture. Aggregate angularity, which can be defined as the measurement of the sharpness of the corners of a particle, has been recognized as a critical property of bituminous mixtures and is one of the primary aggregate properties described in the Superpave specifications. Moreover, angularity is often mentioned as having the potential to influence aggregate and mixture performance through significant interactions with other mixture and material properties. Therefore, the effects of aggregate angularity on mix design characteristics and mixture performance should be appropriately established based on scientific rigor.

Of the various tests for measuring aggregate angularity, the current Superpave mix design method uses the standard "number of fractured faces" testing method (ASTM D5821) for coarse aggregates and the "uncompacted void content" method for fine aggregates (AASHTO T304). Recently, the National Cooperative Highway Research Program (NCHRP) Research Report No. 557 (2006) indicated that current Superpave testing to assess coarse aggregate angularity is empirical and has not been directly related to pavement performance. Based on extensive literature reviews and various testing results, the report found that the uncompacted void content in aggregates reasonably predicts the rutting performance of HMA mixtures better than the current Superpave angularity testing method (i.e., ASTM D5821). In addition, it was specified that an attempt should be made to suggest appropriate testing methods that are more objective, scientific, and reliable to quantify aggregate angularity. For example, numerous state highway agencies and researchers have investigated the Aggregate Imaging System (AIMS). Based on the analysis of two-dimensional images of aggregates, AIMS characterizes angularity by monitoring the difference in the gradient vector measured at various edge points of the

aggregate's image. Interesting correlations have been found between aggregate angularity quantified by AIMS and mixture performance (Masad 2004).

Thus far, a number of studies have been conducted to analyze the effect of aggregate angularity on bituminous mixtures and pavement performance. In their study on the effect of crushed gravel in dense mixtures, Wedding and Gaynor (1961) showed that the use of crushed gravel increased the stability of the asphalt mixture when compared with asphalt mixtures containing uncrushed gravel. Moreover, several studies have indicated that the effect of fine aggregate angularity (FAA) is more significant than that of coarse aggregate angularity (CAA). Foster (1970) studied the resistance of dense-graded hot-mix asphalt mixtures by comparing mixes containing different degrees of crushed and uncrushed coarse aggregates. Although pavement test sections showed similar performance results obtained by the mixes with crushed coarse aggregate and those with uncrushed aggregate, the effect of using fine aggregate was more significant. Cross and Purcell (2001) used mixtures containing natural sand and limestone, and showed that increased FAA results in improved rutting performance. Stiady et al. (2001) evaluated the effect of FAA using the Purdue Laboratory Wheel Track Device (PURWheel) and showed, based on the evaluation of 21 mixtures, that FAA correlated fairly well with performance, although mixtures produced with an FAA higher than 48% did not necessarily perform better than those with an FAA equal to 45%.

Most of the relevant literature has focused on the effect of aggregate angularity on the resistance to permanent deformation and skid resistance (Mahmoud 2005); however, few studies have examined the role of aggregate angularity related to mixture volumetric characteristics and fatigue performance. Compared to the relatively clear benefit of angular particles in rut resistance, mechanical characteristics and related mechanisms on cracking, such as fatigue damage, are not yet fully understood. Furthermore, conflicting results have been reported regarding the effect of the properties of aggregates on the fatigue life of flexible pavement. For example, Huang et al. (1972) reported that the geometric characteristics of coarse aggregates were not significant in the fatigue behavior of asphalt mixtures. By contrast, Maupin (1970) performed a constant strain mode fatigue

test and showed that mixtures containing uncrushed gravel yield better fatigue resistance than mixtures containing crushed limestone or slate.

Therefore, a better and more scientific understanding of the effects of aggregate angularity is necessary, given that the minimum angularity requirements for bituminous mix design significantly affect both mix production costs and long-term pavement performance. Thus, the refinement of aggregate angularity criteria is crucial for state highway agencies and pavement/materials contractors.

1.1. RESEARCH OBJECTIVES

The primary goal of this research is to provide guidelines that potentially help improve current Nebraska asphalt specifications, particularly for aggregate angularity requirements and testing methods based on scientific investigations and experiments. Research outcomes from this study can also be incorporated with research findings from the previous NDOR project (P-556 "*Restricted-Zone Requirements for Superpave Mixes Made with Local Aggregate Sources*"), which will result in a more comprehensive understanding of the effects of aggregate morphology (gradation and angularity) on the performance of asphalt mixtures and pavements in Nebraska.

1.2. RESEARCH SCOPE

To accomplish the objective, this research is divided into four phases. Phase one consists of a literature review, material selection, and volumetric mixture design of target mixtures. The second phase is defined as the evaluation of various aggregate angularity tests, which includes four types of coarse aggregate angularity tests and two fine aggregate angularity tests. The focus of the third phase is the fabrication of asphalt concrete specimens and their mechanical tests to estimate the effects of aggregate angularity on mixture performance characteristics. The static creep test (often referred to as the flow time test) and the asphalt pavement analyzer (APA) test were considered to assess the rutting potential of the mixtures with different angularities, and the indirect

tensile (IDT) test was performed to evaluate fatigue damage characteristics of mixtures with different angularities. The fourth phase of this research is the numerical modeling of the IDT test with finite element simulations of virtual specimens, which attempted to explore the detailed mechanisms of cracking related to the aggregate angularity. Simulation results were then compared with laboratory test results. Based on the experimental test results and numerical simulations, pros and cons of each different angularity testing method are summarized, and the mechanical effects of aggregate angularity on mixture-pavement performance are identified.

1.3. ORGANIZATION OF THE REPORT

This report is composed of five chapters. Following this introduction (Chapter 1), Chapter 2 presents background information found from open literature associated with aggregate angularity, its currently available test methods to assess, and the effect of angularity on mixture-pavement performance. Chapter 3 presents detailed descriptions of material selection and research methodology employed for this study. Chapter 4 shows laboratory test results, such as volumetric mix design results of all mixes, various angularity test results, and mixture performance test results from the APA, static creep, and IDT. Chapter 4 also presents numerical simulation results that model the IDT test to explore the detailed mechanisms of cracking related to the aggregate angularity. Finally, Chapter 5 provides a summary of findings and conclusions of this study. Implementation plans for the Nebraska Department of Roads (NDOR) are also presented in the final chapter.

CHAPTER 2
BACKGROUND

The aggregates' geometry presents three independent characteristics: form, angularity (or roundness), and surface texture. Aggregate angularity can be defined as the measurement of the sharpness of the corners of a particle. Thus, a rounded particle can be classified as a particle with low angularity and a non-rounded particle can be classified as a particle with high angularity. Aggregate form is defined as the variation of the particles' proportion, and the aggregate surface texture is defined based on the irregularities observed from the surface of the particles (Masad 2004). Figure 2.1 (Sukhwani et al. 2006) illustrates geometric characteristics of an aggregate particle to help understand the angularity and other shape features.

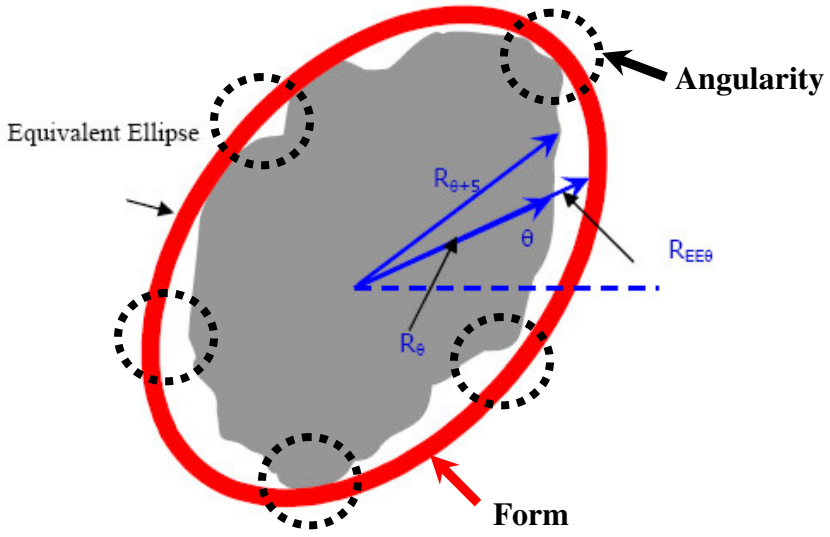

Figure 2.1. Aggregate Shape Characteristics (Sukhwani et al. 2006)

Particle form is quantified by the summation of the incremental changes in a particle radius in all directions. Radius is defined as the length of the line that connects the particle center to points on the boundary. Equation [2.1] gives the form index (*FI*):

$$FI = \sum_{\theta=0}^{\theta=355} \frac{\left|R_{\theta+5} - R_{\theta}\right|}{R_{\theta}} \qquad [2.1]$$

where R = radius of the particle in different directions; and

θ = angle in different directions.

Angularity is analyzed using both the radius and gradient methods. The radius method quantifies angularity by the difference between a particle radius in a certain direction and that of an equivalent ellipse (Figure 2.1). The equivalent ellipse has the same major and minor axes as the particle, but has no angularity. Normalizing the measurements to the radius of an equivalent ellipse minimizes the effect of form on this angularity index. The angularity index using the radius method (AI_R) is expressed as:

$$AI_R = \sum_{\theta=0}^{\theta=355} \frac{R_{\theta} - R_{EE\theta}}{R_{EE\theta}} \qquad [2.2]$$

where R_{θ} = radius of the particle at a directional angle θ; and

$R_{EE\theta}$ = radius of an equivalent ellipse at a directional angle θ.

The gradient method is based on the concept of gradient vectors. The direction of the gradient vector is used to calculate the measure of angularity of aggregate particles. In the gradient method, the direction of the gradient vector for adjacent points changes rapidly at the edge if the corners are sharp. On the other hand, the direction of the gradient vector changes slowly for adjacent points on the edge of the particle for rounded particles. Thus the change in the angle of the gradient vector for a rounded object is much less compared to the change in the angle of gradient vector for an angular object. Angularity values for all the boundary points are calculated and their sum accumulated around the edge to finally form the angularity index of the aggregate particle. The angularity index based on the gradient method (AI_G) is defined as:

$$AI_G = \sum_{i=1}^{n-3} \left| \theta_i - \theta_{i+3} \right| \qquad [2.3]$$

where θ = angle of the gradient vector with the horizontal axis of the image;

i = denotes the ith point on the edge of the particle; and

n = the total number of points on the edge of the particle.

2.1. TEST METHODS TO ESTIMATE AGGREGATE ANGULARITY

Several different types of tests are used to measure aggregate angularity. Currently, the Superpave mix design method requires two standard methods, ASTM D5821 ("Determining Percent of Fractured Particles in Coarse Aggregate) and AASHTO T304 ("Uncompacted Void Content of Fine Aggregate"), to measure coarse and fine aggregate angularities, respectively.

ASTM D5821 is a subjective test that requires the testing operator to evaluate whether the aggregate has fractured faces. The test method cannot distinguish between the angularity of aggregates with 100% two or more fractured faces (most quarried aggregates). As such, NCHRP Project 4-19 (published as NCHRP Report 405: Aggregate Tests Related to Asphalt Concrete Performance in Pavements) (Kandhal et al. 1998) recommended AASHTO TP56 (currently T326), "Uncompacted Voids in Coarse Aggregate," as a replacement. AASHTO T326 combines the effects of aggregate form, angularity, and texture. To date, ASTM D5821, or a similar procedure, is still used by a majority of state agencies.

As mentioned, the Superpave method specifies AASHTO T304 to represent angularity of fine aggregate. The test is to ensure that there is sufficient internal friction—resulting from particle shape, angularity, and texture—to provide rut-resistance in the mixture. The uncompacted voids test is an indirect measure of aggregate shape, angularity, and texture, and works under the assumption that particles that are more flat and elongated, are more

angular, have more texture, or are a combination thereof will not pack as tightly and therefore will have a higher uncompacted void content.

The next group of tests to estimate fine aggregate angularity is to use a compacted specimen subjected to pressure or shear forces. Tests such as a direct shear test, the Florida bearing ratio test, and a compacted aggregate resistance (CAR) test are examples that use compacted specimens. Of these methods, the CAR test is a relatively new test and has not received enough evaluation. Chowdhury and Button (2001) concluded that the CAR test method offers much more sensitivity than the direct shear test. This method also has more advantages than the Florida bearing ratio and direct shear tests.

For the past decade, test methods based on imaging system and analysis have been actively attempted by many researchers for the characterization of aggregate morphology, since the imaging technique can identify aggregates' individual geometric characteristics (i.e., form, angularity, texture, etc.) better and more scientifically than other groups of test methods. Traditional developments include the VDG-40 Videograder, Computer Particle Analyzer, Micromeritics OptiSizer PSDA, Video Imaging System (VIS), and Buffalo Wire Works PSSDA. The VDG-40 Videograder is capable of analyzing every particle in the sample, and it has shown good correlation with manual measurements of flat and elongated particles (Weingart and Prowell 1999; Tutumluer et al. 2000). The PSSDA method is capable of analyzing particles with a wide range of sizes (from passing sieve #200 to 1.5 inches).

The Camsizer system uses two cameras to capture images at different resolutions; it evaluates a large number of particles in the sample as they fall in front of a backlight. Using two cameras improves the accuracy of measuring the characteristics of both coarse and fine aggregates. The system has the capability of automatically producing the distribution of particles' size, shape, angularity, and texture.

The WipShape system uses two cameras to capture images of aggregates passing on a mini-conveyor or on a rotating circular lighting table. This system was selected because it

can analyze large quantities of particles in a short time and has the potential to measure and report various shape factors, including sphericity, roundness, and angularity (Maerz and Lusher 2001; Maerz and Zhou 2001).

The University of Illinois Aggregate Image Analyzer (UIAIA) uses three cameras to capture images from three orthogonal directions and build a 3-D shape of each particle; it automatically determines flat and elongated particles, coarse aggregate angularity, coarse aggregate texture, and gradation. The use of three images for each particle allows an accurate computation of the volume of each aggregate particle and provides information about the actual 3-D characteristics of the aggregate.

Aggregate Imaging System (AIMS) uses one video camera and a microscope to capture different types of images based on the type of aggregate and the property to be measured. The system measures the three dimensions of the aggregate particles. Images can be captured using different resolutions based on the particle size detected by the system. The system is reported to analyze the characteristics of fine and coarse aggregates and provide a detailed analysis of texture for coarse aggregates.

The advantages and disadvantages of various test methods to characterize aggregate angularity are summarized in Table 2.1 (Masad et al. 2007). Each angularity test method can then be categorized into two groups depending on its analysis concept. The first group contains tests that apply a direct approach of angularity measurement, quantifying the angularity through direct measurement of individual particles, and the second group consists of tests that apply an indirect approach of measurement that represent the angularity based on measurements of bulk properties (Masad et al. 2007). Table 2.2 presents the angularity testing methods classified as direct or indirect.

Table 2.1. Advantages and Disadvantages of the Testing Methods Used to Measure Aggregate Characteristics (reproduced from Masad et al. 2007)

Test Method	Measured Aggregate Characteristics	Advantages	Disadvantages
AASHTO T304 (ASTM C1252) Uncompacted Void Content of Fine Aggregate	A combination of angularity, texture, and shape	1. Simple 2. Inexpensive 3. Used in the current Superpave system	1. The test does not consistently identify angular and cubical aggregates. 2. The results are influenced by shape, angularity, texture, and bulk specific gravity.
AASHTO T326 Uncompacted Void Content of Coarse Aggregate	A combination of angularity, texture, and shape	1. Simple 2. Inexpensive	1. The results are influenced by shape, angularity, texture, and bulk specific gravity.
ASTM D3398 Standard Test Method for Index of Aggregate Particle Shape and Texture	A combination of angularity, texture, and shape	1. Simple 2. Inexpensive	1. The method does not provide good correlation with concrete performance. 2. Results are influenced by bulk properties, shape, angularity, and texture.
Compacted Aggregate Resistance (CAR) Test	A combination of angularity, texture, and shape	1. Simple 2. Inexpensive 3. More sensitive to changes in aggregate characteristics than FAA and direct shear methods.	1. The results are influenced by shape, angularity, texture, and bulk properties.
Florida Bearing Value of Fine Aggregate	A combination of angularity, texture, and shape	1. Simple	1. The results are influenced by shape, angularity, texture, and bulk properties. 2. Less practical and involves more steps than the FAA. 3. Operates based on the same concept as the CAR test but requires more equipment and time.
AASHTO T236 (ASTM D3080) Direct Shear Test	A combination of angularity, texture, and shape	1. Simple 2. Test method has good correlation with HMA performance.	1. Expensive 2. The results are influenced by shape, angularity, texture, mineralogy, and particle size distribution. 3. Nonuniform stress distribution causes discrepancies in the measured internal friction.
ASTM D5821 Determining the Percentages of Fractured Particles in Coarse Aggregate	Angularity	1. Simple 2. Inexpensive 3. Used in the current Superpave system	1. Labor intensive and time consuming 2. Depends on the operator's judgment. 3. Provides low prediction, precision, and medium practicality.
Flat and Elongated Coarse Aggregates (ASTM D4791)	Shape	1. Used in the current Superpave system 2. Able to identify large portions of flat and elongated particles 3. Gives accurate measurements of particle dimension ratio.	1. Tedious, labor intensive, time consuming to be used on a daily basis. 2. Limited to test only one particle at a time. 3. Unable to identify spherical, rounded, or smooth particles. 4. Does not directly predict performance.

Table 2.1. Continued

Test Method	Measured Aggregate Characteristics	Advantages	Disadvantages
VDG-40 Videograder	Shape	1. Measures the shape of large aggregate quantity. 2. Good correlation with manual measurements of flat-elongated particles	1. Expensive 2. Does not address angularity or texture. 3. Assumes idealized particle shape (ellipsoid). 4. Uses one camera magnification to capture images of all sizes.
Computer Particle Analyzer (CPA)	Shape	1. Measures the shape of large aggregate quantity.	1. Expensive 2. Does not address angularity or texture. 3. Assumes idealized particle shape (ellipsoid). 4. Uses one camera magnification to capture images of all sizes.
Micrometrics OptiSizer PSDA	Shape	1. Measures the shape of large aggregate quantity.	1. Expensive 2. Does not address angularity or texture. 3. Assumes idealized particle shape (ellipsoid). 4. Uses one camera magnification to capture images of all sizes.
Video Imaging System (VIS)	Shape	1. Measures the shape of large aggregate quantity.	1. Expensive 2. Does not address angularity or texture. 3. Assumes idealized particle shape (ellipsoid). 4. Uses one camera magnification to capture images of all sizes.
Camsizer	Shape and Angularity	1. Measures the shape of large aggregate quantity. 2. Uses two cameras to capture images at different magnifications based on aggregate size.	1. Expensive 2. Assumes idealized particle shape (ellipsoid).
WipShape	Shape and Angularity	1. Measures the shape of large aggregate quantity. 2. Measures the three dimensions of aggregates.	1. Expensive 2. Does not address texture. 3. Uses same camera magnification to capture images of all sizes.
University of Illinois Aggregate Image Analyzer (UIAIA)	Shape, Angularity, and Texture	1. Measures the shape of large aggregate quantity. 2. Measures the three dimensions of aggregates.	1. Expensive 2. Uses same camera magnification to capture images of all sizes.
Aggregate Imaging System (AIMS)	Shape, Angularity, and Texture	1. Measures the three dimensions of aggregates. 2. Uses a mechanism for capturing images at different resolutions based on particle size. 3. Gives detailed analysis of texture.	1. Expensive
Laser-Based Aggregate Analysis System	Shape, Angularity, and Texture	1. Measures the three dimensions of aggregates.	1. Expensive 2. Use the same scan to analyze aggregates with different sizes.

Table 2.2. Features of Test Methods for Experimental Evaluation (reproduced from Masad et al. 2007)

Test Method	Direct (D) or Indirect (I) Method	Features of Analysis Concept
AASHTO T304 (ASTM C1252) Uncompacted Void Content of Fine Aggregate	I	Packing of aggregate that flows through a given sized orifice
AASHTO T326 Uncompacted Void Content of Coarse Aggregate	I	
ASTM D3398 Standard Test Method for Index of Aggregate Particle Shape and Texture	I	Packing of aggregate in a mold using two levels of compactions
Compacted Aggregate Resistance (CAR) Test	I	Exposing a compacted specimen to pressure or shear forces
Florida Bearing Value of Fine Aggregate	I	
AASHTO T236 (ASTM D3080) Direct Shear Test	I	
ASTM D5821 Determining the Percentages of Fractured Particles in Coarse Aggregate	D	Visual inspection of particles
Flat and Elongated Coarse Aggregates (ASTM D4791)	D	Measuring particle dimension using caliper
VDG-40 Videograder	D	Using one camera to image and evaluate particles in the sample as they fall in front of a back light
Computer Particle Analyzer (CPA)	D	
Micrometrics OptiSizer PSDA	D	
Video Imaging System (VIS)	D	
Camsizer	D	Uses two cameras to image and evaluate particles in the sample as they fall in front of a back light
WipShape	D	Uses two cameras to capture image of aggregates passing on a mini conveyor system
University of Illinois Aggregate Image Analyzer (UIAIA)	D	Uses three cameras to capture three projections of a particle moving on a conveyor belt
Aggregate Imaging System (AIMS)	D	Uses one camera and autofocus microscope to measure the characteristics of coarse and fine aggregates
Laser-Based Aggregate Analysis System	D	Uses a laser scan

2.2. EFFECT OF AGGREGATE ANGULARITY ON HMA PERFORMANCE

Cross and Brown (1992) studied the effects of aggregate angularity on the rutting potential based on testing conducted on 42 pavements in 14 states; 30 of the 42 pavements had experienced premature rutting. Rut-depth measurements and cores were taken at each site. The cores were tested for their aggregate characteristics, such as the percent with two crushed faces and the uncompacted void content. Data analysis indicated that there is a relationship between the percent with two crushed faces in the coarse aggregate and the rutting rate when in-place air voids were greater than 2.5%, while none of the aggregate properties were related to the rutting rate when air voids were less than 2.5%.

Kandhal and Parker (1998) evaluated the properties of nine coarse aggregate sources by performing nine tests to evaluate coarse aggregate shape, angularity, and texture. Rut testing was also performed on the mixtures using the Superpave Shear Tester (SST) and Georgia Loaded Wheel Tester (GLWT). The uncompacted voids in the coarse aggregate test (AASHTO T326) produced the best relationships with the rutting parameters from all nine mixtures. The results from AASHTO T326 and ASTM D3398 ("Index of Aggregate Particle Shape and Texture") were highly correlated.

Hand et al. (2000) conducted round-robin testing to determine the precision of ASTM D5821. The study was initiated because of concerns that insufficient fractured faces in the original crushed gravel source used at WesTrack may have contributed to the premature failure of the coarse-graded sections. The materials were collected from cold feed samples taken during the construction and reconstruction of WesTrack. Four materials were included in the study. By monitoring the percentage of fractured faces of the mixtures considered, the study concluded that coarse aggregate angularity did not have an effect on the rutting performance of Superpave mixtures at WesTrack.

A Canadian study (2002) was conducted in Saskatchewan to investigate the effect of the percentage of fractured coarse aggregate particles on rutting performance with 10

pavements ranging in age from two to nine years. Rut depths were measured and cores were recovered within and between the wheel paths. Cores were tested for density, voids filled, asphalt content, coarse aggregate fractured face count, and uncompacted void content in fine aggregate. A stepwise regression was performed to identify the factors most related to the in-place rut depth. Regression analysis between the reported fractured face counts and rutting rate indicated no clear relationship.

Ahlrich (1996) investigated 11 aggregate blends. The blends were produced by combining different percentages of crushed limestone, crushed gravel, uncrushed gravel, and natural sand. The blends were combined to produce 0%, 30%, 50%, 70%, and 100% crushed coarse aggregate particle counts. The resulting mixtures were tested for rutting resistance using a confined repeated-load permanent deformation test. Coarse aggregate shape, angularity, and texture were evaluated using the test for fractured face count, ASTM D3398, and the uncompacted voids in coarse aggregate test (AASHTO T326). Testing indicated a strong correlation between the individual tests and parameters from the confined repeated-load permanent deformation test. The combined (coarse and fine aggregate) particle index value from ASTM D3398 appears to provide the best overall correlation with the rutting performance results.

Full-scale rutting tests were performed at the Indiana Department of Transportation (DOT) accelerated pavement testing (APT) facility in West Lafayette, Indiana (Rismantojo 2002). Five mixes were tested in the APT facility. The rounded gravel mix produced 29.5 mm of rutting after 5,000 passes, at which time testing was terminated. The other four sections containing quarried 18 stone were tested to 20,000 passes. A strong relationship was identified between the uncompacted voids and the total rut depth at 5,000 passes. This relationship is strongly influenced by the uncrushed gravel mixture. When the gravel mix is excluded and only the four mixes that were tested to 20,000 passes are analyzed, the uncompacted voids in the coarse aggregate performed on the plant stockpile material produces the best correlation.

As introduced, numerous studies have indicated improved rut resistance with increased coarse aggregate angularity. Furthermore, several other studies have evaluated the relationship between both the particle index value (ASTM D3398) and the coarse aggregate uncompacted voids test (AASHTO T326) and rutting performance. Trends indicate that higher particle index values or uncompacted void contents produce more rut-resistant pavements.

Stuart and Mogawer (1994) conducted a study to evaluate different methods of measuring fine aggregate shape and texture. Twelve materials were evaluated in the study—five natural sands with a poor performance history, four natural sands with a good performance history, and three manufactured (crushed) sands with a good performance history—by performing five different laboratory tests, including the uncompacted voids test, ASTM D3398, and a flow time test to characterize mixture rutting potential. The 12 sands were ranked by each of the test methods based on the average test value. The best method of differentiation was the flow time test. ASTM D3398 correctly differentiated all of the poor-quality sands from the good-quality sands. The weighted particle index that divided good- and poor-performing materials was between 11.7 and 13.9. Later, Mogawer and Stuart (1992) concluded that 44.7% uncompacted voids would divide good- and poor-performing sands for high traffic levels.

Huber et al. (1998) conducted a study to assess the contribution of fine aggregate angularity and particle shape to the rutting performance of a Superpave-designed asphalt mixture. Four fine aggregates were selected for the study: Georgia granite, Alabama limestone, Indiana crushed sand, and Indiana natural sand. The uncompacted void contents (AASHTO T304) of the four aggregates were measured as 48, 46, 42, and 38, respectively. A reference mixture was prepared with the Georgia granite (coarse and fine aggregate) and a PG 67-22 binder. The other three aggregates were sieved into size fractions and substituted for the granite fine aggregate to produce four mixtures, keeping the gradation constant. All four blends were mixed at the optimum asphalt content determined for the granite blend. The resulting mixtures were tested in the Couch Wheel Tracker (a modified Hamburg Wheel Tracker), the Asphalt Pavement Analyzer (APA),

and the SST using the frequency sweep test. The rutting tests did not appear to differentiate between the blends in a consistent manner—or at all, in some cases. The authors concluded that the choice of coarse aggregate might have masked the effect of the fine aggregate. There was not a clear correlation between any of the tests and the uncompacted void contents.

NCHRP Project 4-19, "Aggregate Tests Related to Asphalt Concrete Performance in Pavements," (Kandhal and Parker 1998) evaluated fine aggregate tests related to rutting performance. Three tests were used in the study: ASTM D3398, AASHTO T304, and particle shape from image analysis (the University of Arkansas method). Used in this study were nine fine aggregate sources with a range in uncompacted void contents of 40.3% to 47.5%. Three of the materials were natural sands. The fine aggregates were mixed with an uncrushed gravel coarse aggregate. All of the mixes were produced using the same gradation, above the maximum density line. The coarse aggregate and gradation were chosen to emphasize the response of the fine aggregate. The resulting mixtures were tested using the GLWT and the SST. Poor correlation coefficients were observed between all three fine aggregate tests and the SST results. The index of aggregate shape and particle texture from ASTM D3398 produced the best correlation with the GLWT rut depths. The uncompacted void contents produced a slightly lower correlation. The authors recommended AASHTO T304 to quantify fine aggregate particle shape, angularity, and surface texture due to its simplicity and high correlation with the aggregate index.

Lee et al. (1999) conducted a study on the effect of fine aggregate angularity on asphalt mixture performance for the Indiana DOT. The study included six fine aggregate sources, which were used to produce different gradations and blends. The angularity of the fine aggregates were evaluated, which resulted in the uncompacted void content of the fine aggregate ranging from 38.7 to 49.0. Volumetric mix designs were conducted, and rut testing was also performed on the mixtures using the PurWheel Laboratory Tracking Device and the SST. Correlation analysis between the fine aggregate tests and rutting performance based on both repeated shear at constant height and the PurWheel rut depths

indicated that the uncompacted void content was highly correlated with rutting performance. The authors however concluded that uncompacted voids alone may not be sufficient to evaluate the fine aggregate contribution to mixture rutting performance. It was observed that a mixture having an uncompacted void content of 43 performed as well as a mixture with an uncompacted void content of 48. The authors noted that this may be due to the confounding effects of gradation and compactability.

National Pooled Fund Study No. 176 (Haddock et al. 1999), "Validation of SHRP Asphalt Mixture Specifications Using Accelerated Testing," was conducted to examine the effect of fine aggregate angularity on the rutting performance of Superpave mixtures. Two coarse aggregates (a limestone and granite) and three fine aggregates (a natural sand, limestone sand, and granite sand) were used in the study. The fine aggregates had uncompacted void contents of 39%, 44%, and 50%, respectively. The rutting propensities of the mixes were tested with the PurWheel, the SST, and Triaxial Tests and in the APT facility. In Phase II of the project, an additional six mixtures were tested in the APT facility for a total of 10 mixtures. Stiady et al. (2001) discussed the findings obtained from the project relative to aggregate. The rounded natural sand (uncompacted void content of 39%) produced the worst rutting performance; however, the limestone fine aggregate (uncompacted void content of 44%) performed as well or better than the granite fine aggregate (uncompacted void content of 50%). Analysis of variance (ANOVA) performed on the triaxial shear strength test results indicated that the uncompacted void contents for the fine aggregates in the mixtures were a significant factor (Hand et al. 2001).

Chowdhury et al. (2001) conducted a study to evaluate various measures of fine aggregate angularity and texture and their relationship to rutting performance. The study evaluated 23 fine aggregates using seven different procedures: uncompacted void content (AASHTO T304), ASTM D3080, CAR test, three different methods of digital image analysis, and visual inspection. A laboratory rutting study was conducted with four of the fine aggregates: three crushed materials and one natural sand. Cylindrical samples at 4 ± 1% air voids were tested in the APA at 64°C. Regression analysis indicated a fair to

poor relationship between uncompacted voids and APA rut depth. The mix with 100% natural sand fines (uncompacted void content of 39%) had the highest rut depth, followed closely by the mix with the crushed river gravel fines (uncompacted void content of 44.3%). The mix with the granite fines (uncompacted void content of 48%) had the least amount of rutting, followed closely by the mix with the limestone fines (uncompacted void content of 43.5%). Laboratory results imply that it is possible to design mixes using fine aggregate that fails the uncompacted voids criteria but produces acceptable rutting performance.

Roque et al. (2002) conducted a study on fine aggregate angularity for the Florida DOT. A total of nine fine aggregates were included in the study: six limestone sources, two granite sources, and a gravel source. The fine aggregates were evaluated visually and using AASHTO T304 and ASTM D3080. A poor correlation was observed between the uncompacted void content and direct shear strength. The trend indicates decreasing shear strength with increasing uncompacted void content. This may be due to the packing characteristics of the fine aggregates with higher uncompacted void contents. The authors concluded that "although fine aggregate angularity had some influence on the shear strength, aggregate toughness and gradation appeared to overwhelm its effects, confirming that fine aggregate angularity alone was not a good predictor of fine aggregate shear strength." Rutting tests were also performed with the APA. The trend between uncompacted voids and APA rut depths indicated decreased rutting with increasing uncompacted voids.

Stackston et al. (2002) conducted a study to evaluate the effect of fine aggregate angularity on compaction effort and rutting resistance. Three aggregate sources were used in the study. Twenty-four Superpave mix designs were developed using blends of the three materials and two gradation shapes: fine and s-shaped. The response of the mixtures was evaluated using Superpave volumetric properties and the gyratory load plate assembly. The gyratory load plate assembly measures the force on the sample at three points. Testing indicated that the density at $N_{initial}$ decreases with increasing uncompacted void content. This indicates that mixes with higher uncompacted void contents would be

less likely to be tender mixes. Data from the gyratory load plate assembly indicated that mixes with higher uncompacted void contents are harder to compact. The authors reported that the effect of uncompacted void content was not consistent in terms of rutting resistance as measured by the gyratory load plate assembly.

NCHRP Project 4-19 (Kandhal and Parker 1998) examined the relationship between uncompacted void tests and rutting through accelerated testing using the Indiana prototype APT facility. Six fine aggregates were initially selected for the fine aggregate characterization portion of the study: crushed gravel, granite, dolomite, traprock sands, and two natural sands. The uncompacted void contents for these sands ranged from 40.3% to 49.1% (Rismantojo 2002). The six mixtures with passing Superpave volumetric properties were tested in the full-scale Indiana APT facility. The results indicate that uncompacted voids were significantly related to the total rut depth after 1,000 passes. The author noted that the decrease in rut depth with increasing uncompacted voids occurs to a lesser extent above 45% voids. Rismantojo (2002) concluded that the results of the study are similar to those reported by Kandhal and Parker (1998), including that fine-graded mixtures with uncompacted void contents between 42% and 46% demonstrate similar levels of rutting resistance.

The results of various studies relating the uncompacted void content (representing fine aggregate angularity) to performance are mixed. Generally, studies indicated a trend between uncompacted void content and improved rutting performance, but in some cases the trend was weak. Subtle differences in uncompacted void content can be overwhelmed by the effect of the coarse aggregate or other mixture properties. Several studies supported the 45% uncompacted void criteria for high traffic, but several also indicated performance was unclear between 43% and 45% (or higher) uncompacted voids. There is clear evidence that good-performing mixes can be designed with uncompacted void contents between 43% and 45%, but evaluation of these mixes using a rutting performance test is recommended. Furthermore, higher uncompacted void contents generally resulted in lower densities at $N_{initial}$.

CHAPTER 3
RESEARCH METHODOLOGY

This chapter describes materials used in this research (aggregates, asphalt binder, and an anti-stripping additive, hydrated lime). It also illustrates mix design methods to obtain five Superpave mixes with different combinations of coarse aggregate angularity (CAA) and fine aggregate angularity (FAA) values. Then, a brief description of laboratory tests included in this study is presented. Several different test methods to estimate CAA and FAA were conducted in this study. Characteristics and concepts of each angularity test method are briefly introduced in this chapter. Then, three laboratory performance tests (i.e., the uniaxial static creep test, the asphalt pavement analyzer (APA) test, and the indirect tensile fracture energy test) involved in this research to investigate mixtures' rutting and fatigue-cracking resistance are described. The indirect tensile fracture energy test employed two different asphalt mixtures: the asphalt concrete mixture to evaluate both CAA and FAA effects, and the fine aggregate asphalt matrix mixture for particularly evaluating the effect of FAA. Results from the indirect tensile fracture energy test were then incorporated with finite element simulations of virtual specimens that were attempted to explore the detailed mechanisms of cracking related to the aggregate angularity.

3.1. MATERIALS SELECTION

To accomplish a more realistic simulation of asphalt mixtures paved in Nebraska, the most widely used local paving materials (aggregates and asphalt binder) were selected for fabricating laboratory samples. In addition, an anti-stripping agent, hydrated lime was used in this project, since hydrated lime has been used as an active anti-stripping agent for pavements constructed in Nebraska due to its unique chemical and mechanical characteristics.

3.1.1 Aggregates

A total of seven types of local aggregates (5/8-inch limestone, 1/4-inch limestone, screenings, 2A, 3ACR-LA, 3ACR-HA, and 47B) were used in this study. These aggregates were selected because they are the most widely used by Nebraska pavement contractors. Table 3.1 illustrates laboratory-measured physical properties, such as bulk specific gravity (G_{sb}) and absorption capacity of each aggregate. In addition, important Superpave aggregate consensus properties, coarse aggregate angularity (CAA), fine aggregate angularity (FAA), and sand equivalency (SE) are also presented in the table. As can be seen, each aggregate demonstrates very different characteristics; therefore, a wide range of aggregate blends meeting target specific gravity and angularity can be obtained via appropriate aggregate mixing. For this study, aggregates were blended in order to obtain mixes with desired values of CAA (75%, 90%, and 97%) and FAA (43.5% and 45.5%).

Table 3.1. Fundamental Properties of Aggregates

	Aggregate Property						
	Fine Aggregate				**Coarse Aggregate**		
Material	G_{sb}	**Absorption Capacity (%)**	**FAA (%)**	**Sand Equivalency (%)**	G_{sb}	**Absorption Capacity (%)**	**CAA (%)**
5/8" LS	-	-	-	-	2.624	1.25	100.0
1/4" LS	-	-	-	-	2.607	1.54	100.0
Screening	2.478	3.66	46.7	26.0	-	-	-
2A	2.580	0.76	37.6	100.0	2.589	0.68	28.0
3ACR-LA	2.556	1.13	43.7	84.0	2.588	0.75	91.0
3ACR-HA	2.576	1.13	45.7	84.0	-	-	-
47B	2.605	0.49	37.3	98.0	2.594	0.65	35.0

3.1.2. Asphalt binder

The asphalt binder used in this project is a Superpave performance-graded binder PG 64-28 provided from Flint Hills, located in Omaha, Nebraska. This type of binder has been mostly used for low-traffic-volume roads in Nebraska. Table 3.2 present fundamental properties of the binder by performing dynamic shear rheometer (DSR) tests and bending beam rheometer (BBR) tests, which have been designated in the Superpave binder specification to identify performance grade and viscoelastic properties of asphalt binder.

Table 3.2. Asphalt Binder Properties of PG 64-28

Test	Temperature (^oC)	Test Result	Required Value
Unaged DSR, $\|G^*\|/\sin\delta$ (kPa)	64	1.494	min. 1.00
Unaged phase angle (degree)	64	74.76	-
RTFO - elastic recovery	25	74	-
RTFO, Aged DSR $\|G^*\|/\sin\delta$ (kPa)	64	3.445	min. 2.20
PAV - Aged DSR, $\|G^*\|\sin\delta$ (kPa)	22	3,245	max. 5,000
PAV - Aged BBR, stiffness (Mpa)	-18	240	max. 300
PAV - Aged BBR, *m*-value	-18	0.306	min. 0.30

3.1.3. Hydrated lime

The use of hydrated lime has been recommended in Nebraska, where asphalt pavements are susceptible to moisture-related stripping. Hydrated lime has been known to be an effective material to reduce moisture damage of pavements due to its unique physical-chemical-mechanical characteristics. Hydrated lime was obtained from Mississippi Lime Company, located in Sainte Genevieve, Missouri. Tables 3.3 and 3.4 illustrate the basic physical and chemical properties of hydrated lime used for this study.

Table 3.3. Physical Properties of Hydrated Lime

Physical Properties	
Specific Gravity	2.343
Dry Brightness, G.E.	92.0
Median Particle Size - Sedigraph	2 micron
pH	12.4
BET Surface Area	22 m^2/g
-100 Mesh (150 µm)	100.0%
-200 Mesh (150 µm)	99.0%
-350 Mesh (150 µm)	94.0%
Apparent Dry Bulk Density – Loose	22lbs./ft^3
Apparent Dry Bulk Density – Packed	35lbs./ft^3

Table 3.4. Chemical Properties of Hydrated Lime

Chemical Properties	
$CA(OH)_2$ – Total	98.00%
$CA(OH)_2$ – Available	96.80%
CO_2	0.50%
H_2O	0.70%
$CaSO_4$	0.10%
Sulfur – Equivalent	0.024%
Crystaline Silica	<0.1%
SiO_2	0.50%
Al_2O_3	0.20%
Fe_2O_3	0.06%
MgO	0.40%
P_2O_5	0.010%
MnO	0.0025%

3.2. MIX DESIGN METHOD

Five Superpave mixtures were designed to conduct the indirect tensile fracture energy and the uniaxial static creep tests. In order to evaluate the effect of aggregate angularity on the asphalt mixture performance, three CAA values (75%, 90%, and 97%) and two FAA values (43.5% and 45.5%) were selected to produce five combinations as presented in Table 3.5. The selection of angularity values was based on the analysis of field asphalt pavement projects carried out over the last decade in Nebraska. The chosen values were the most common angularity values used in the field. Each mixture was designed to find its optimum asphalt content until all volumetric parameters of the mixtures met the required Nebraska Superpave specifications. All five mixes, designed in the Geomaterials Laboratory at the University of Nebraska–Lincoln (UNL), were submitted to NDOR asphalt/aggregate laboratories for validation of aggregate properties (i.e., Superpave consensus properties of aggregates) and volumetric mix design parameters. Figure 3.1 presents a gradation of aggregate blends targeted to form each mix. As shown in the figure, the mix is located below the restricted zone and contains 3.5% of mineral filler—aggregates passing the No. 200 sieve (0.075-mm mesh size).

Table 3.5. Five Mixtures Designed for This Study

Mixtures	Angularity Characteristics
Mix 1	CAA = 97%, FAA 45.5%
Mix 2	CAA = 90%, FAA 45.5%
Mix 3	CAA = 75%, FAA 45.5%
Mix 4	CAA = 90%, FAA 43.5%
Mix 5	CAA = 75%, FAA 43.5%

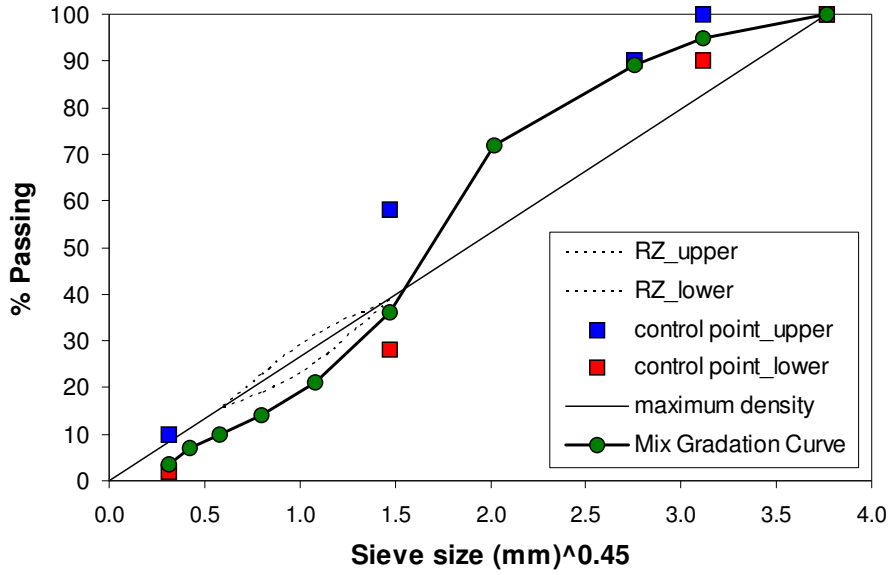

Figure 3.1. A Target Gradation Curve of Aggregate Blends

The five asphalt concrete mixtures were produced in order to achieve the 4% ± 1% air voids requirement of Superpave methodology, and for that reason, different percentages of binder content were necessary for each mixture. This indicates that two variables, aggregate angularity and binder content, are involved in the analysis of asphalt concrete performance test results, which may be misleading the understanding of the pure effect of aggregate angularity on mixture performance. Thus, to obtain mixtures where the same binder content is maintained but different angularity values are applied, two fine

aggregate matrix (FAM) mixtures targeting different FAA values (43.5 and 45.5) were also produced. The FAM mixture is defined herein as the combination of asphalt binder and aggregates passing through sieve No. 16 (mesh size of 1.18 mm). As illustrated in Figure 3.2, the FAM mixture gradation was obtained from the original mixture gradation shown in Figure 3.1, excluding the aggregates larger than 1.18 mm (i.e., retained on sieve No. 8). Since the FAM mixtures contain only fine aggregates, volumetric characteristics such as air voids between two mixtures were not significantly different, even if the same amount of asphalt binder (6.0% in this study) was used. This implies that the effect of FAA on mixture performance can be observed in a much more efficient way than using asphalt concrete mixture results. The amount of binder, 6.0%, was determined as an appropriate value that guarantees complete coating of aggregates with no bleeding on the completion of mixture compaction. Figure 3.3 compares the internal microstructure of the FAM mixture and the asphalt concrete mixture, respectively.

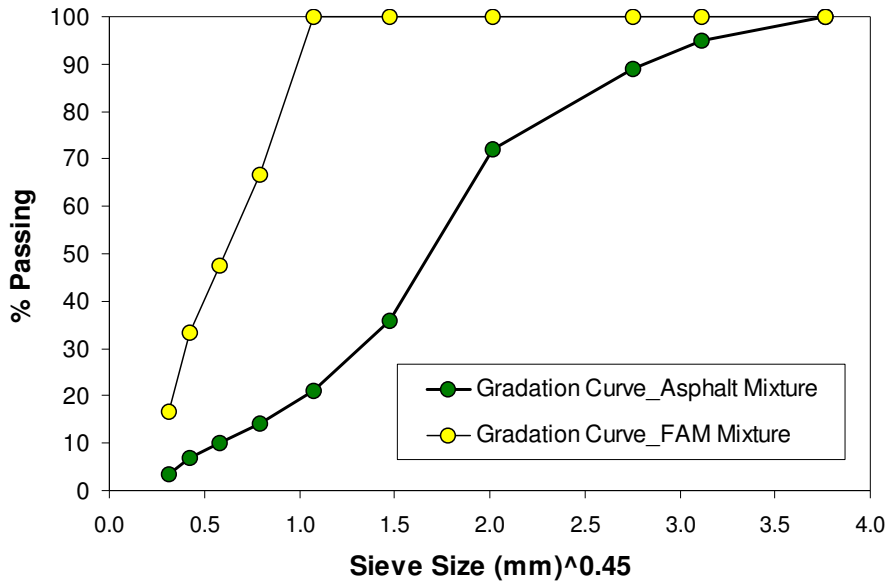

Figure 3.2. Gradation Curves of the Asphalt Mixtures and the FAM Mixtures

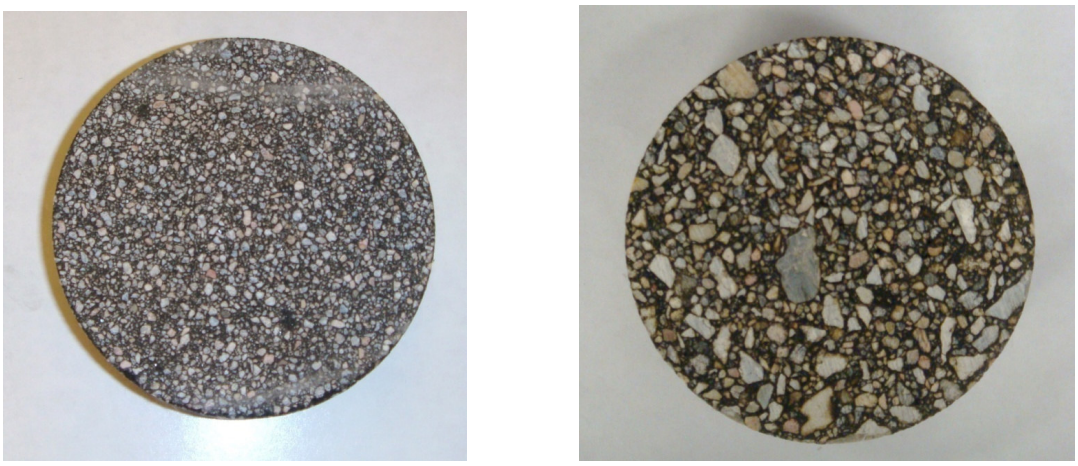

(a) (b)

Figure 3.3. Internal Microstructure of (a) FAM Mixture; (b) Asphalt Concrete Mixture

3.3. AGGREGATE ANGULARITY TESTS PERFORMED

Several different angularity test methods were estimated in this study. In this section, each test method is briefly described. Test results are presented in the next chapter.

3.3.1. Coarse aggregate angularity (CAA) tests

Four different test methods characterizing CAA values were evaluated: ASTM D5821 ("Determining Percent of Fractured Particles in Coarse Aggregate), which is the most widely used standard method to date; AASHTO T326 ("Standard Method of Test for Uncompacted Void Content of Coarse Aggregate"), which has not yet been adopted by many state agencies but has gained increasing attentions; and the two image analysis methods: the Aggregate Imaging System (AIMS) approach that has been recently developed to be a unified method characterizing aggregate morphology (shape, size, angularity, and texture), and a simple two-dimensional (2-D) digital image process and analysis that uses ImageTool, public domain image analysis software.

3.3.1.1. ASTM D5821 Method

ASTM D5821 was based on the Pennsylvania test method and was later adopted as the method for measuring coarse aggregate angularity within the Superpave mix design method. The fractured face count of a representative sample of coarse aggregate is determined by visual inspection. ASTM D5821 (2002) defines a fractured face as "an angular, rough, or broken surface of an aggregate particle created by crushing, by other artificial means, or by nature." A face is considered fractured only if it has the projected area of fractured face (A_f) greater than 25% of the maximum particle cross-sectional area (X_{max}), as illustrated in Figure 3.4. A fractured particle is "a particle of aggregate having at least the minimum number of fractured faces specified (usually one or two)" (ASTM D5821 2002).

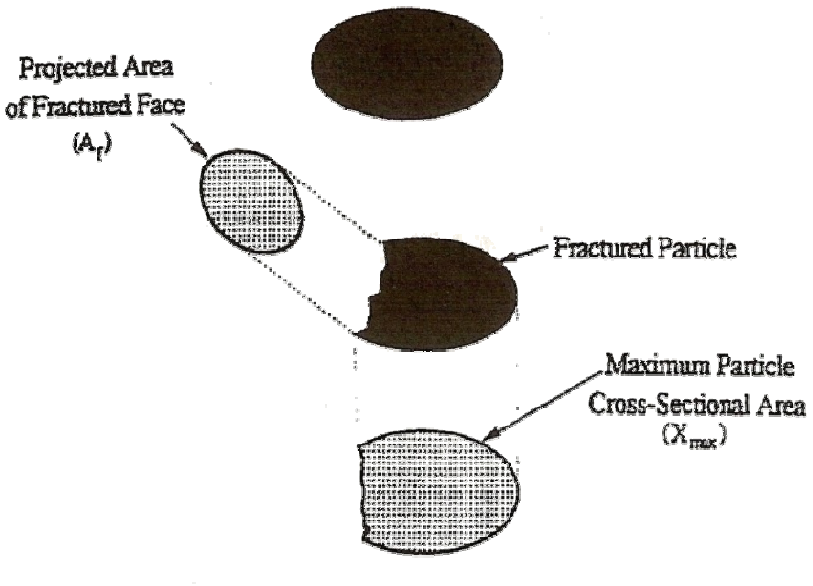

Figure 3.4. Definition of Fractured Face (ASTM D5821 2002)

To run the test, a representative sample is washed over the 4.75-mm sieve and dried to a constant mass. The size of the sample is dependent on the nominal maximum aggregate size (NMAS) of the aggregate. The aggregate particles are visually inspected and divided into piles of particles with no fractured faces and one or more fractured faces. After all of the particles are sorted, the mass of each pile is determined. The percentage of fractured particles is expressed as the mass of particles having a given number of fractured faces divided by the total mass of the samples (result expressed as a percentage), as mathematically expressed in Equation [3.1].

$$P(\%) = \frac{F}{F+N} * 100 \qquad [3.1]$$

where P = percentage of particles with the specified number of fractured faces;

F = mass or count of fractured particles with at least the specified number of fractured face; and

N = mass or count of particles in the nonfractured category not meeting the fractured face criterion.

For Superpave specifications, after the percentage of particles with one or more fractured faces is determined, the aggregates are reexamined for two or more fractured faces. Figure 3.5 illustrates two distinct groups of aggregates: aggregates classified as nonfractured face and classified as fractured face aggregates.

(a) non-fractured face (b) fractured face

Figure 3.5. Aggregates with Different Angularity Characteristics

3.3.1.2. AASHTO T326 Method

Ahlrich (1996) developed the uncompacted voids in coarse aggregate test based on ASTM C1252, "Uncompacted Void Content in Fine Aggregate." Both AASHTO T326 and ASTM C1252 use the same concept to quantify the aggregate angularity; the higher the percentage of voids, the higher the angularity of the aggregate, as illustrated in Figure 3.6. AASHTO T326 is preferable to ASTM D5821 because it requires much less testing time to perform; however, the effects of particle shape, angularity, and texture cannot be purely separated, since the uncompacted void content of coarse aggregates is directly or indirectly related to all three aggregate characteristics: shape, angularity, and texture. The apparatus used to perform this test is presented in Figure 3.7.

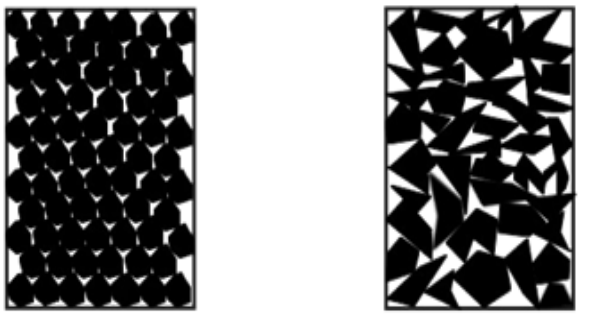

(a) low angularity (b) high angularity

Figure 3.6. Correlation between Aggregate Angularity and Voids

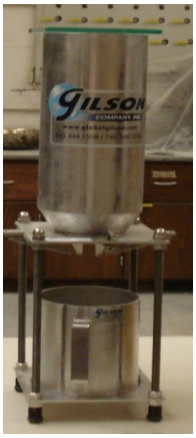

Figure 3.7. Apparatus of the AASHTO T326 Test

3.3.1.3. Aggregate Imaging System (AIMS)

The AIMS method was developed by researchers at Texas A&M University. The AIMS contains both a fine aggregate and a coarse aggregate module (Masad 2003). These two modules allow the system to capture measurements of shape (form), angularity, and texture altogether. The system (Figure 3.8) consists of a video microscope, video camera, data acquisition system, lighting system, automated carriage, and associated software. The aggregate particles are randomly spread on a disk tray. A video microscope is coupled with a black-and-white video camera to acquire images. The images are then analyzed to identify aggregates' angularity, form, and surface texture characteristics. The most recent AIMS device manufactured by Pine provides software (shown in Figure 3.9) that produces image analysis results in spreadsheet (such as Microsoft Excel) files so that users can easily manipulate test data.

(a) Exterior View (b) Inside of the Chamber

Figure 3.8. AIMS Device

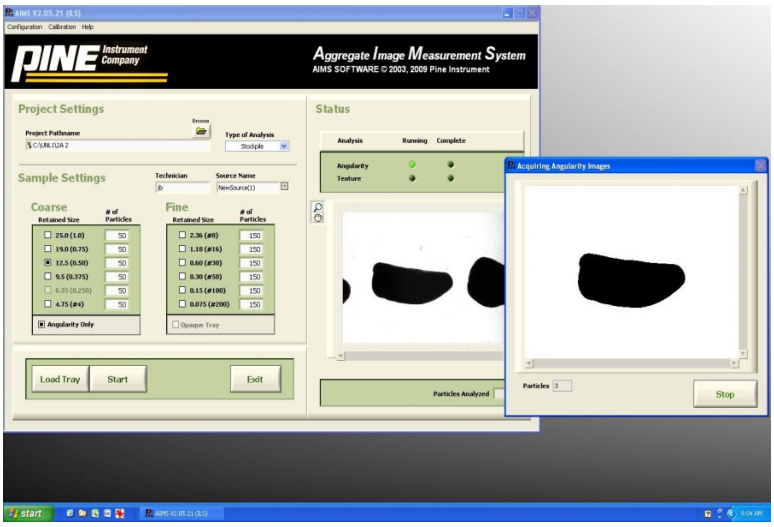

Figure 3.9. AIMS Interface for Coarse Aggregates

Evaluation of aggregate angularity is based on the analysis of two-dimensional (2-D) image of aggregates by monitoring differences of the gradient vectors at different edge points of the aggregate image. The gradient vector is obtained at the edge of the particle image, and its direction is determined based on the changing of colors from white (aggregate) to black (background), as shown in Figure 3.9. Simply, the concept is that at smooth corners of the image, the gradient vector changes slowly, while at sharp corners it changes rapidly (Bathina 2005). Figure 3.10 exemplifies the concept with two cases: a rounded particle and an angular particle. Clearly, the change in the gradient vectors in the angular particle is much more rapid than the change from the rounded particle. The angularity index (AI_G) can then be calculated from the accumulated sum of the difference of consecutive gradient vectors for all edge points (Masad 2004) as presented in Equation [2.3] in the previous chapter.

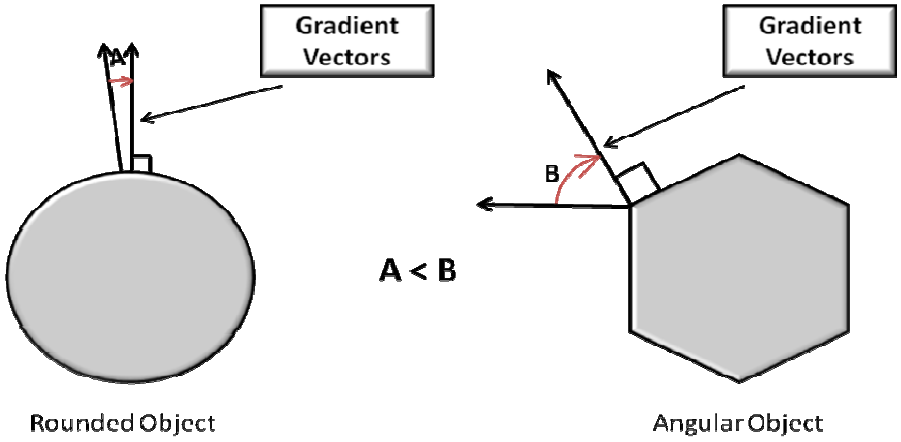

Figure 3.10. AIMS Gradient Method to Quantify Angularity

3.3.1.4. Two-dimensional Digital Image Process and Analysis

The two-dimensional (2-D) digital image analysis was also evaluated in this study as a potential approach to estimate coarse aggregate angularity since it is very simple, fast, and economical to perform. For the testing, digital image creation and processing of aggregate particles are performed following a set of steps, and then the processed image is analyzed by using public domain software (ImageTool) that was developed by the University of Texas Health and Science Center. As illustrated in Figure 3.11, the digital image processing is typically composed of four steps: digital image formation, image enhancement, segmentation, and identification of the objects.

Digital image formation is the first step in any digital image processing application. From this step, the aggregates are simply digitalized using a conventional scanner. Then, image enhancement techniques are applied to highlight certain characteristics of interest in the image. Enhancement is a simple but very subjective area of image processing, because enhancement is based on human subjective preferences depending on what features of the image is important to the analysis (Gonzalez and Woods 2008). Figure 3.11(b) shows the image of aggregates transformed in black and white. This step can be executed using a commercial image editor such as CorelDraw or Photoshop. Next step is segmentation,

which is the detection of object boundaries, as presented in Figure 3.11(c). This step is performed by using edge- and line-detection techniques. Segmentation is considered one of the most critical tasks in digital image processing (Gonzalez and Woods 2008), because this step involves recognizing and separating the object of interests from the background. The segmentation was executed by using the ImageTool software. After the detection of object boundaries through the segmentation process, the next step is the identification of the objects. This stage provides specific geometric characteristics, such as perimeter, area, and roundness, of each identified object. Figure 3.11(d) illustrates the process performed by the ImageTool software.

(a) image formation

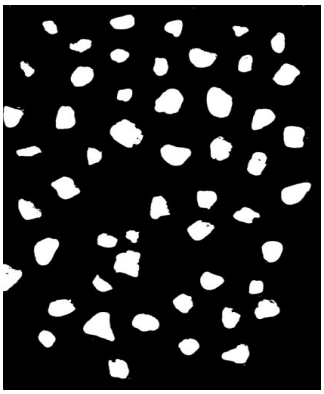

(b) image enhancement

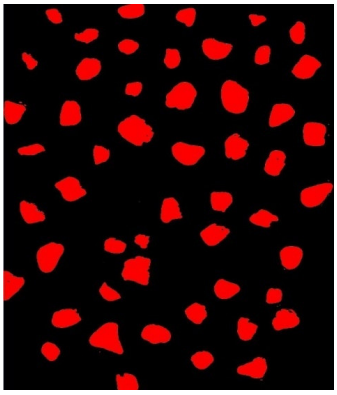

(c) image segmentation

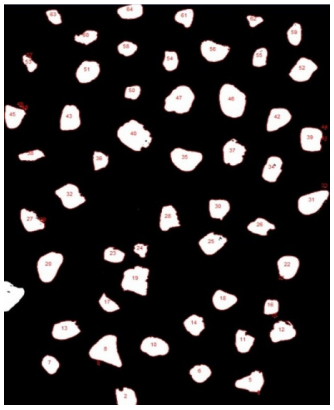

(d) identification of objects

Figure 3.11. Steps of the Two-Dimensional Digital Image Processing

The roundness parameter resulting from the digital image analysis is used as an angularity measurement. The roundness is between 0 and 1, where the greater the value, the rounder the object. The roundness can be calculated as follows:

$$roundness = \frac{4 * \pi * A}{P^2} \quad [3.2]$$

where A = area of the particle image; and

P = perimeter of the particle image.

3.3.2. Fine aggregate angularity (FAA) tests

Among several different testing methods to evaluate fine aggregate angularity, two tests were analyzed in this study: AASHTO T304 ("Uncompacted Void Content of Fine Aggregate"), which is the most widely used method designated in the current Superpave specification; and the AIMS approach, which is a method that has been receiving increasing attention from the asphalt pavement community due to its more scientific characteristics.

3.3.2.1. AASHTO T304 Method

AASHTO T304 is commonly referred to as the FAA test. The Superpave method specifies AASHTO T304 to ensure that the blend of fine aggregates in an asphalt mixture has sufficient internal friction to provide rut-resistance in the mixture (McGennis et al. 1994), since higher internal friction is typically associated with increased rutting resistance. The amount of friction depends on the aggregate particle shape and texture. AASHTO T304 test is an indirect measure of particle shape, angularity, and texture, since it is based on an empirical observation indicating that more angular particles or particles with more surface texture are not packed together as tightly as rounded or smooth particles would be.

As presented in Figure 3.12, a 190-g sample of fine aggregate of a prescribed gradation is allowed to flow through the orifice of a funnel and fill a 100-cm^3 calibrated cylinder. Excess material is struck off, and the cylinder with aggregate is weighed. The

uncompacted void content of the sample is then computed using the loosely compacted weight of the aggregate, the bulk dry specific gravity of the aggregate, and the calibrated volume of the receiving cylinder. Equation [3.3] presents a mathematical formula to calculate the uncompacted void content in fine aggregates. The FAA value is defined as the percentage of air voids in a loosely compacted sample of fine aggregate.

$$U(\%) = \frac{V - \left(\frac{F}{G}\right)}{V} * 100 \qquad [3.3]$$

where U = uncompacted void content (in percentage);

V = known volume of the cylinder;

F = net mass (in gram) of fine aggregates; and

G = bulk specific gravity of fine aggregate sample.

Figure 3.12. AASHTO T304 Testing Apparatus

There are three methods for running AASHTO T304: Methods A, B, and C. The mass of the sample for all three methods is fixed at 190 g. Method A specifies a known gradation ranging from material passing the 2.36-mm sieve to material retained on the 0.15-mm

sieve. Method B specifies that the test be run on three individual size fractions: 2.36 to 1.18 mm, 1.18 to 0.60 mm, and 0.60 to 0.30 mm. The reported void content for Method B is the average of the results from the three individual size fractions. In Method C, the test is run on the as-received gradation. The Superpave researchers chose Method A to limit the effect of gradation, particularly material passing the 0.075-mm sieve on the test result.

3.3.2.2. Aggregate Imaging System (AIMS)

This test uses the same device shown in Figure 4.5. Measurement concept is also based on the changes of the gradient vector on the edges of the particle image, as described in section 3.3.1.3. The only difference between the test procedure for fine aggregates and the one for coarse aggregates is the amount of particles for each sieve size. Table 3.6 presents the suggested number of particles presented in the operator's manual.

Table 3.6. Sample Size of AIMS for Fine Aggregates

Sieve Size	Suggested Number of Particles
Coarse Aggregate	
12.5 mm (1/2")	50
9.5 mm (3/8")	50
4.75 mm (#4)	50
Fine Aggregate	
2.36 mm (#8)	150
1.18 mm (#16)	150
0.6 mm (#30)	150
0.3 mm (#50)	150
0.15 mm (#100)	150
0.075 mm (#200)	150

Similar to the coarse aggregate case, the image of individual fine aggregate particle is analyzed to identify its angularity and form characteristics. The most recent AIMS system manufactured by Pine provides a user-friendly interface (shown in Figure 3.13), and test results are summarized in Excel spreadsheets for further graphing and data analyses.

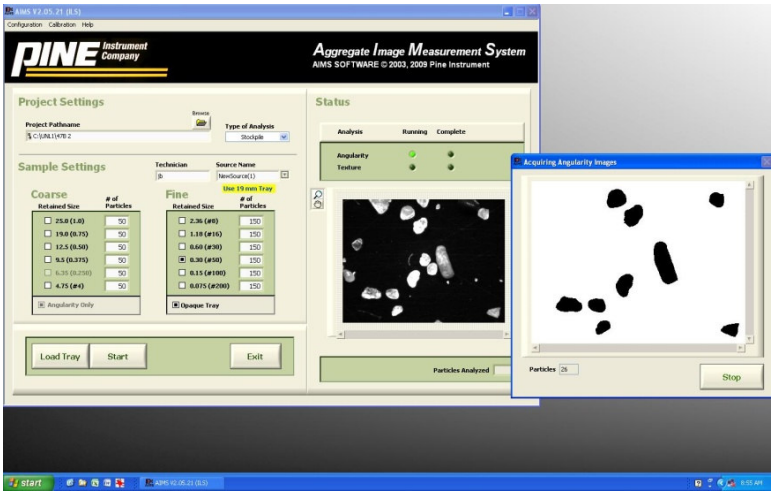

Figure 3.13. AIMS Interface for Fine Aggregates

3.4. PERFORMANCE TESTS OF MIXTURES

The effect of aggregate angularity on mixture performance was investigated by conducting laboratory performance tests (the uniaxial static creep test and the indirect tensile fracture energy test) of five mixes designed with different combinations of coarse and fine aggregate angularity and statistical analyses of five-year asphalt pavement analyzer (APA) test results of field mixtures. The indirect tensile fracture energy test employed two different asphalt mixtures: the asphalt concrete mixture to evaluate both CAA and FAA effects, and the fine aggregate asphalt matrix mixture for particularly evaluating the effect of FAA. For the all mechanical performance tests (except the APA test), the UTM-25kN (Universal Testing Machine with a 25-kN loading capacity) mechanical testing system, installed in the UNL Geomaterials Laboratory, was used.

3.4.1. Uniaxial static creep test

The uniaxial static creep test was performed to assess the rutting resistance of each mixture. In this test, cylindrical specimens were subjected to static axial loads, and the applied stress and strain responses were recorded throughout the test. The test procedure including the sample fabrication process is described in the NCHRP report No. 465 (Witczak et al. 2002).

A Superpave gyratory compactor was used to produce the cylindrical samples with a diameter of 150 mm and an approximate height of 170 mm. Then, the samples were cored and sawed to produce testing specimens with a 100-mm diameter and 150-mm height. Figure 3.14 presents a specimen after the compaction and coring-sawing process.

Figure 3.14. A Specimen Cored and Sawed from the Gyratory Compacted Sample

To measure the axial displacement of the specimen under the constant compressive force, mounting studs were fixed to the surface of the specimen with epoxy glue so that the three linear variable differential transformers (LVDTs) could be attached onto the surface of the specimen at 120^{o} radial intervals with a 100-mm gauge length, as illustrated in Figure 3.15. Then, the specimen was mounted in the UTM-25kN testing station for the testing (Figure 3.16).

Figure 3.15. A Device Used to Place the Mounting Studs for LVDTs

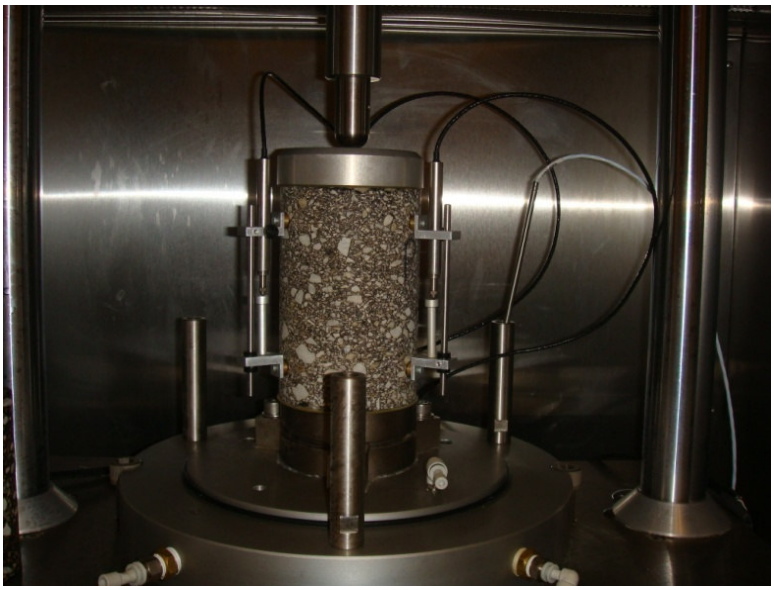

Figure 3.16. A Specimen with LVDTs Mounted in the UTM-25kN

The static creep test was conducted on three replicas of each type of mixture at 60°C. A constant pressure of 207 kPa (30 psi) was applied to the specimens, and the vertical deformation (in compression) was monitored with the three LVDTs. Figure 3.17 shows a typical relationship between the calculated vertical deformation and loading time. As shown, the total deformation can be divided into three major zones:

1. The primary zone—the portion in which the deformation rate decreases with loading time;
2. The secondary zone—the portion in which the deformation rate is constant with loading time; and
3. The tertiary flow zone—the portion in which the deformation rate increases with loading time.

The failure point due to plastic flow is determined at the transition stage from secondary creep to tertiary creep. The starting point of the tertiary zone was defined as the flow time and is considered a very good evaluation parameter of the rutting resistance of asphalt concrete mixtures (Hafez 1997).

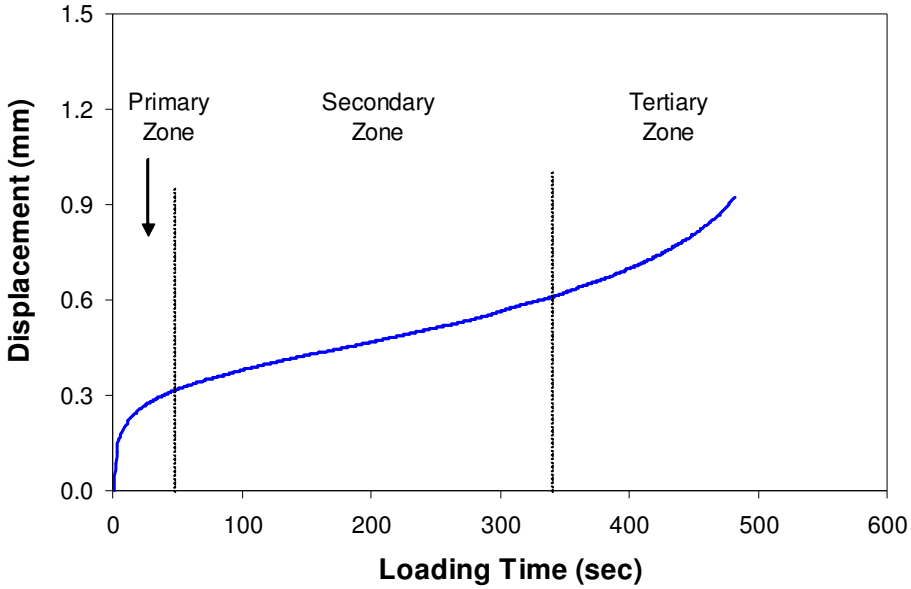

Figure 3.17. Typical Test Results of the Uniaxial Static Creep Test

3.4.2. Asphalt pavement analyzer (APA) test

Rutting susceptibility of asphalt concrete samples can be practically evaluated using the APA testing equipment shown in Figure 3.18. The APA is an automated, new generation of the Georgia Load Wheel Tester (GLWT) used to evaluate rutting, fatigue, and moisture resistance of asphalt concrete mixtures. During the APA test, the rutting susceptibility of compacted specimens is tested by applying repetitive linear loads through three pressurized hoses via wheels to simulate trafficking. Even though it has been reported that APA testing results are not very well correlated with actual field performance, APA testing is relatively simple to perform and produces a ranking of mixtures' rutting potential by simply measuring sample rut depth.

(a) APA with Beam and Cylindrical Samples

(b) Front View of APA

Figure 3.18. Asphalt Pavement Analyzer (APA)

In addition to the uniaxial static creep test, the APA test was considered to assess the effect of aggregate angularity on a mixture's rutting potential. Instead of performing the APA test for the five mixtures shown in Table 3.5, APA test data accumulated in the NDOR laboratory were obtained and used for this study. This approach might be somewhat limited to provide a direct relationship between the aggregate angularity and the mixture's rutting potential, because many other variables are involved in the process; however, a simple statistical analysis of the test results obtained from various types of Nebraska asphalt mixes (i.e., *SP-2*, *SP-4*, *SP-4S*, and *SP-5*) is expected to produce at least some useful insights into the role of aggregate angularities to the mixtures' rutting performance.

The number of APA specimens considered was 11, 90, 24, and 21 for *SP-2*, *SP-4*, *SP-4S*, and *SP-5*, respectively. Asphalt field mixtures were compacted in the laboratory to produce testing specimens, 150 mm in diameter and 50 mm high. For all specimens, the hose pressure and wheel load were 690 kPa and 445 N (100 psi and 100 lb), respectively. All tests were performed at 64^{o}C.

3.4.3. Indirect Tensile Fracture Energy Test

To evaluate the effects of aggregate angularity on fatigue damage resistance, the indirect tensile (IDT) test was performed on laboratory mixed, laboratory compacted specimens. As in several studies (Kim et al. 2002; Wen and Kim 2002; Kim and Wen 2002) conducted at North Carolina State University, the fracture energy obtained from the IDT test can be a good indicator for field performance. In the studies, the ranking of the mixtures with respect to this parameter agreed with that of the mixtures in the field, with respect to the percentage of fatigue cracking, as illustrated in Figure 3.19 (Kim et al. 2002). They validated the use of fracture energy by testing actual pavement cores; that is, the field mixed–field compacted specimens and fracture energy was able to distinguish between the performance of mixtures with different gradations, asphalt contents, and air void contents.

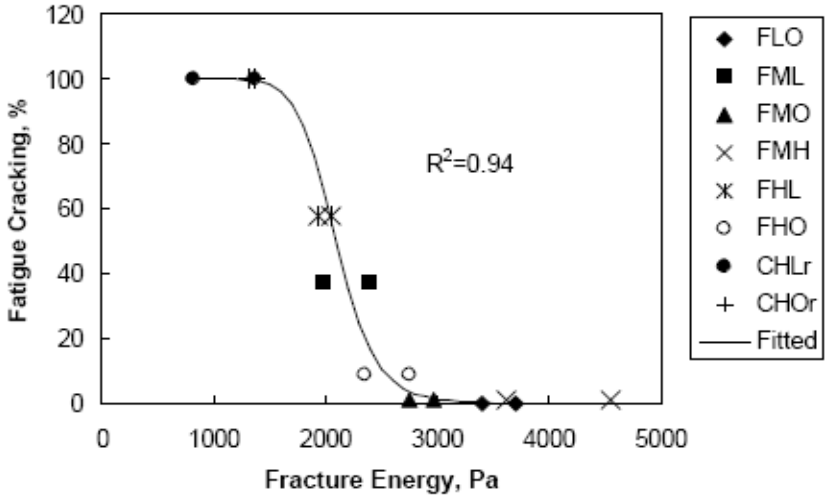

Figure 3.19. Relationship between Field Fatigue Performance and IDT Fracture Energy (Kim et al. 2002)

In addition, the IDT test is easy to perform and can significantly reduce testing efforts compared to typical mixture fatigue tests. Typical fatigue tests require long testing times, and test results are usually not repeatable.

Following the procedures described in Kim et al. (2002), Superpave gyratory compacted samples of 150-mm diameter and approximately 115-mm tall were produced and then cored to produce specimens with a diameter of 100 mm. Each cored specimen was then cut to produce two IDT specimens 38-mm tall, as shown in Figure 3.20. Then, gauge points were glued over a 50-mm gauge length in the center of the specimen on both faces to measure horizontal and vertical displacements during the IDT fracture test. The gauge points were placed as accurately as possible on the desired locations of the specimen to alleviate positioning errors. Toward the end, a gauge-point mounting and gluing device, as shown in Figure 3.21, was developed and used. Lateral metallic bars were also used to avoid rotation and translation at the top and bottom plates while gluing the gauge points.

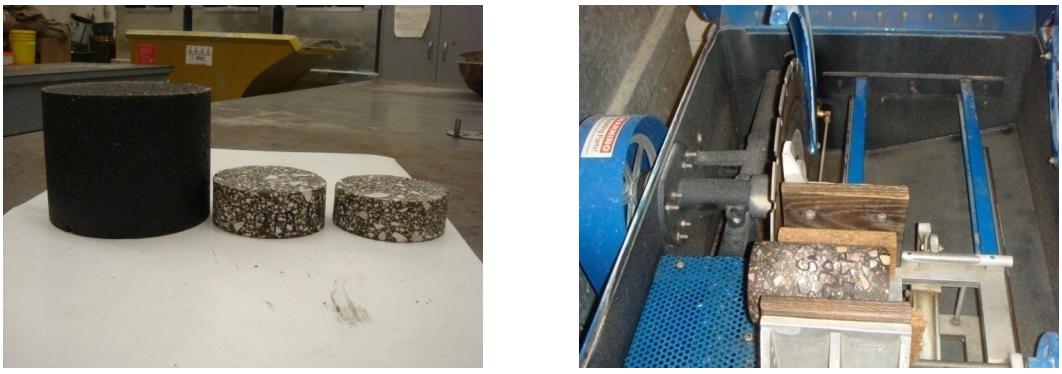

Figure 3.20. Testing Specimens after Coring-Sawing Process

Figure 3.21. Gauge-Point Mounting Device

Then, the specimen was mounted in the UTM-25kN testing station (as shown in Figure 3.22). A constant crosshead rate loading (0.833 mm/s) was applied to the specimen at 20°C. Horizontal and vertical displacements were measured from the cross LVDTs on both faces.

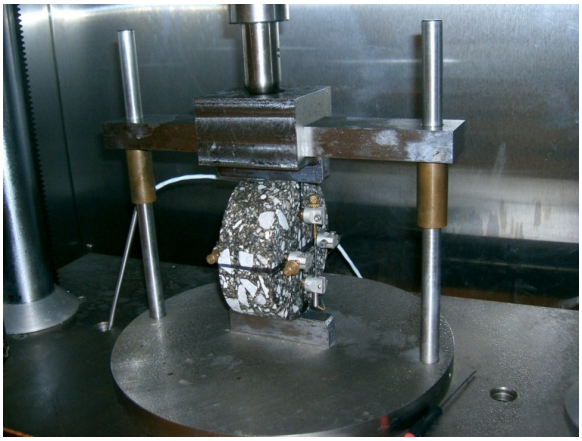

Figure 3.22. An IDT Specimen Installed in the UTM-25kN

Using the horizontal displacements measured, the strain is calculated at the center of the specimen using the following equation.

$$\varepsilon_{x=0}(t) = U(t)\frac{\gamma_1 + \nu\gamma_2}{\gamma_3 + \nu\gamma_4} \qquad [3.5]$$

where $\varepsilon_{x=0}(t)$ = strain at the center;

$U(t)$ = horizontal displacement (m);

$\gamma_1, \gamma_2, \gamma_3, \gamma_4$ = parameters; and

ν = Poisson's ratio (0.35).

The parameters γ_1, γ_2, γ_3, and γ_4 are related to specimen diameter and gauge length used. Table 3.7 shows the values of these parameters for specimens with different diameters

and gauge lengths (Kim et al. 2002). Since the IDT specimens for this study used 100-mm diameter and 50.8-mm gauge length, the parameters γ_1, γ_2, γ_3, and γ_4 are 12.4, 37.7, 0.471, and 1.57, respectively.

Table 3.7. Parameters in Equation [3.5]

Specimen Diameter (mm)	Gauge Length (mm)	γ_1	γ_2	γ_3	γ_4
100	25.4	12.4	37.7	0.291	0.908
100	50.8	12.4	37.7	0.471	1.57
150	25.4	8.48	27.6	0.207	0.634
150	50.8	8.48	27.6	0.378	1.18
100	76.2	8.48	27.6	0.478	1.59

The stress at the center of the specimen can also be calculated based on the equation developed by Hondros (1959), which is written as follows:

$$\sigma_{x=0}(t) = \frac{2P(t)}{\pi t d} \qquad [3.6]$$

where $\sigma_{x=0}(t)$ = strain at the center;

$P(t)$ = force applied;

t = thickness of the specimen (38 mm in this study); and

d = diameter of the specimen (100 mm in this study).

Using Equations [3.5] and [3.6], test results can then be plotted in a stress-strain curve, as illustrated in Figure 3.23. The area under the stress-strain curve until peak stress is defined as the fracture energy (Kim et al. 2002).

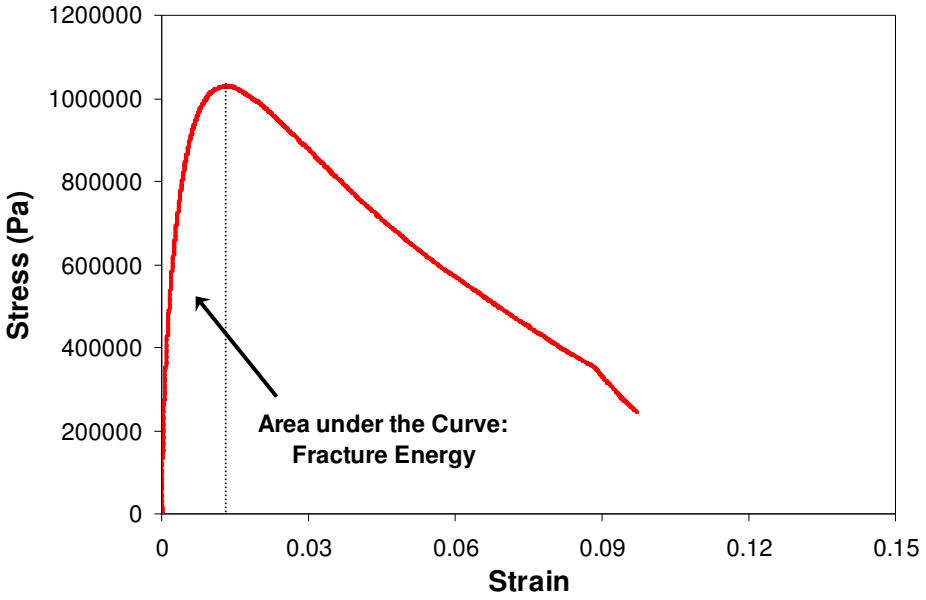

Figure 3.23. Typical Stress-Strain Plot of the IDT Fracture Test

3.5. FINITE ELEMENT MODELING OF IDT FRACTURE TESTING

The objective of this effort is to further investigate the effect of aggregate angularity through a numerical modeling approach. Some visible findings and related inferences can be obtained from the results of the indirect tensile test; however, the global behavior observed from the laboratory test is not often sufficient to address the detailed local events occurring in the specimens. Angularity, a material-level (aggregate) design variable, is one of critical properties of bituminous mixtures and is regarded as having the potential to influence mixture performance through a significant level of interactions with other materials such as binders. Thus, the effects of aggregate angularity on mixture performance would be better identified by certain approaches that can provide insights into detailed local behavior and interactions among materials.

Recently, a micromechanics-based computational modeling approach has been actively pursued to account for the effects of individual mixture constituents (e.g., aggregates and asphalt binder) on overall mixture performance. Some studies (Masad et al. 2001;

Papagiannakis et al. 2002; Dai and You 2007) have proposed finite element (FE) method-based models to characterize the damage performance of asphaltic composites. The discrete element method (DEM), an explicit numerical technique, has also been employed by several researchers (Abbas and Shenoy 2005; You and Buttlar 2006; You et al. 2008). These computational approaches allow engineers to better understand the mechanical effects of small-scale design variables (such as asphalt mastic film thickness, air voids in the mix, size/shape/distribution of aggregates, mineral additives in the mixture, volume fraction of asphalt mastics, etc.) on overall damage-associated responses and the lifetimes of mixtures.

To this end, the micromechanical FE simulation was implemented in this study to investigate in greater detail the effect of angularity on asphalt mixture fatigue performance. Modeling and simulations were carried out using a UNL in-house code that has been developed and employed to model various composite materials and structures (Kim et al. 2006a, 2006b, 2007). The code is based on the FE method and incorporates elasticity, viscoelasticity, and nonlinear fracture. Since asphalt mixtures consist of elastic aggregates and viscoelastic asphalt, and typically present nonlinear viscoelastic fracture, all of these features are essentially necessary for the modeling of asphalt mixtures. The indirect tensile fracture energy test was simulated using this code. The same loading condition (a constant displacement rate of 0.833 mm/s) was applied to all modeled specimens.

3.5.1. Finite element mesh

In order to accomplish micromechanical FE modeling, it is necessary to construct and mesh the internal microstructure of the specimen. For this study, the inner microstructure of the specimens was artificially generated by a newly developed virtual microstructure generator (Souza 2009). The virtual microstructure generator allows the experimental effort to be considerably reduced due to its virtual mixture fabrication and laboratory testing. The current working (beta) version of the virtual microstructure generator can produce the microstructure of mixtures with known basic geometric properties of aggregates (i.e., gradation, angularity, elongation, and orientation) and mixture

volumetric parameters (such as volume fraction of each phase). In particular, the angularity characteristic is controlled by its input aggregate imaging system (AIMS) values of aggregate particles. Figure 3.24 exemplifies several internal microstructures virtually generated.

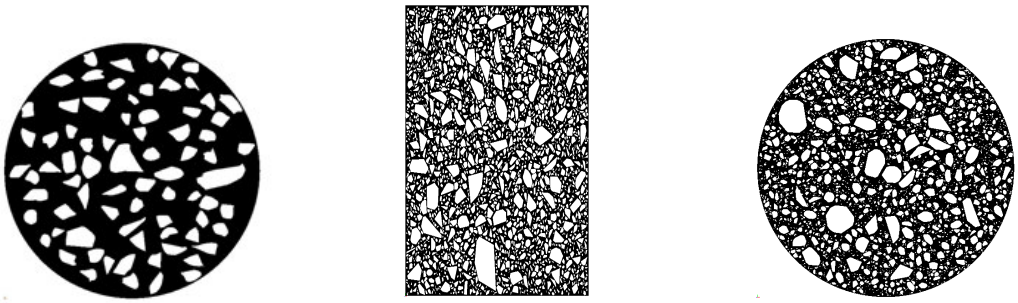

(a) (b) (c)

Figure 3.24. Several Internal Microstructures Virtually Generated

With the virtually generated microstructure, triangular elements were used for the FE meshing, as presented in Figure 3.25, which is the FE mesh of Figure 3.24(c). It can be noted that a higher degree of refinement was intended around the aggregates in order to capture more accurately any detailed mechanical behavior related to angularity. In addition, studies of mesh and time step convergence were performed to minimize numerical errors. Analysis results indicate that a time step of 0.01 second and a mesh with 15,000 elements were adequate to guarantee a reasonable degree of accuracy.

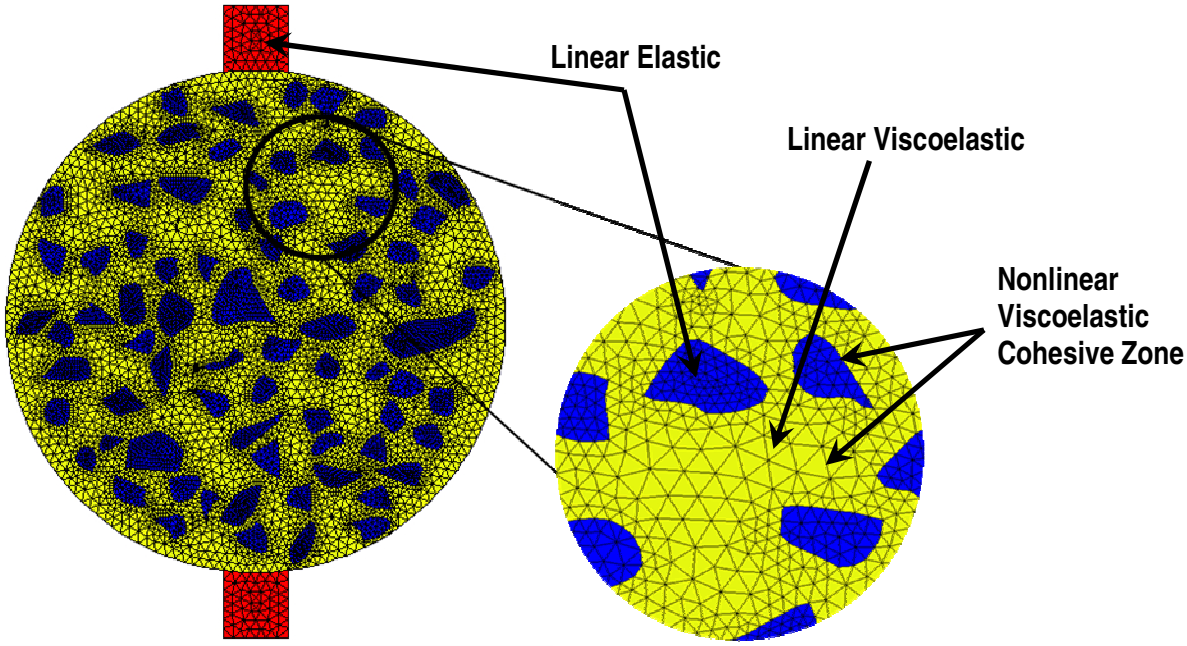

Figure 3.25. Finite Element Mesh of the Virtual Specimen

3.5.2. Modeling methodology

Figure 3.25 also presents the constitutive relation of each phase for the FE modeling. As shown in the figure, aggregates and metal blocks (loading strips) were modeled as linear elastic materials. The linear elastic constitutive relationship can be expressed as:

$$\sigma_{ij}(x_m,t) = C_{ijkl,E}\varepsilon_{kl}(x_m,t) \qquad [3.7]$$

where $\sigma_{ij}(x_m,t)$ = stress as a function of space and time;

$\varepsilon_{kl}(x_m,t)$ = strain as a function of space and time;

$C_{ijkl,E}$ = elastic modulus, which is not time-dependent;

x_m = spatial coordinates; and

t = time of interest.

The time-independent elastic modulus consists of elastic material properties. If the individual particle of aggregates and the metal loading strips are assumed to follow

simply isotropic linear elastic behavior, only two independent material constants among Young's modulus (E), shear modulus (G), and Poisson's ratio (ν) are required.

The constitutive behavior of the asphalt phase surrounding aggregates can often be represented by the following linear viscoelastic convolution integral:

$$\sigma_{ij}(x_m,t) = \int_0^t C_{ijkl,VE}(t-\tau)\frac{\partial \varepsilon_{kl}(x_m,\tau)}{\partial \tau}d\tau \qquad [3.8]$$

where $C_{ijkl,VE}(t)$ = linear viscoelastic time-dependent stress relaxation modulus; and

τ = time-history integration variable.

The linear viscoelastic relaxation modulus of the asphalt phase is often represented by a mathematical form such as a Prony series based on the generalized Maxwell model. The linear viscoelastic stress relaxation modulus by a Prony series can be expressed as:

$$C_{ijkl,VE}(t) = C_{ijkl,\infty} + \sum_{p=1}^{M} C_{ijkl,p}\exp\left(-\frac{t}{\rho_{ijkl,p}}\right) \qquad [3.9]$$

where $C_{ijkl,\infty}$ and $C_{ijkl,p}$ = spring constants in the generalized Maxwell model;

$\rho_{ijkl,p}$ = relaxation times in the generalized Maxwell model; and

M = the number of dashpots in the generalized Maxwell model.

To simulate cracking and fracture failure, the cohesive zone concept was implemented in the modeling. Fracture behavior can be modeled in many different ways, and one of the well-known approaches is to use the cohesive zone. Cohesive zone approaches regard fracture as a gradual phenomenon in which separation takes place across an extended crack tip, or cohesive zone (fracture process zone), and where the fracture is resisted by cohesive tractions. As shown in Figure 3.26, cohesive zones are placed between continuum elements to represent the progressive separation of a material. The cohesive zone effectively describes the material resistance when material elements are being displaced.

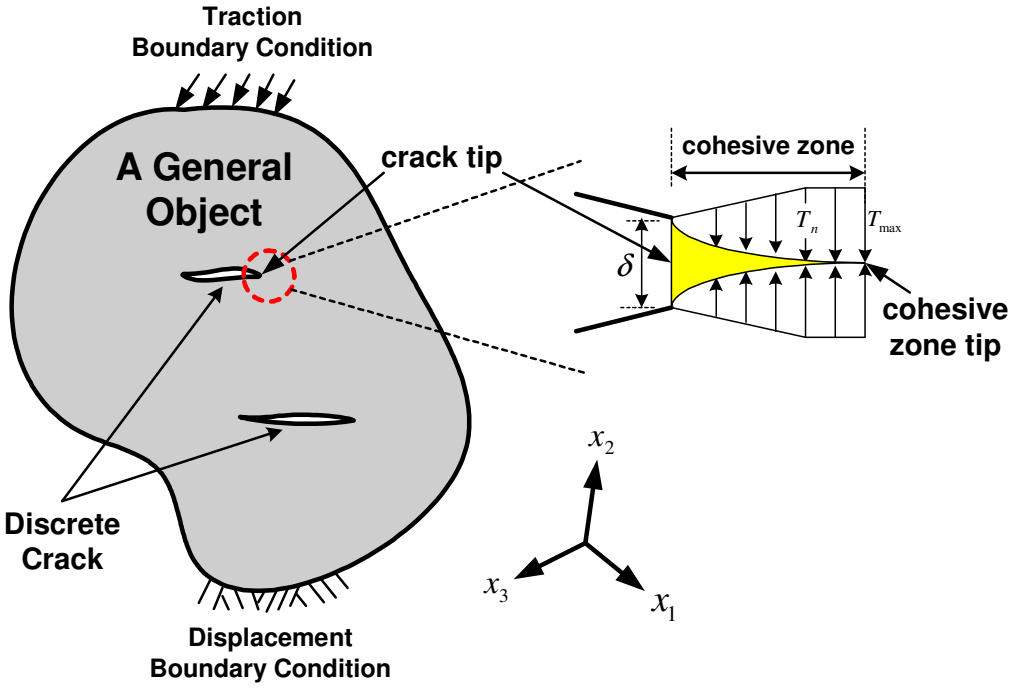

Figure 3.26. Schematic Representation of the Cohesive Zone Concept

Cohesive zone models are well-established tools in classic fracture mechanics developed to remove stress singularities ahead of crack tips. Recently, the cohesive zone concept has been employed in several studies, most of which attempted to simulate crack-associated fracture damage of asphalt concrete mixtures (Song et al. 2006; Kim et al. 2007. Among the various cohesive zone models available, this study used a cohesive zone model developed by Allen and Searcy (2001), because the model can reflect nonlinear viscoelastic damage growth in the asphalt mixtures. Furthermore, the model can predict damage evolution, microcracking, corresponding post-peak material softening, and eventual fracture failure of highly inelastic asphalt mixtures. The general traction-displacement relationship for the nonlinear viscoelastic cohesive zone model is as follows (Allen and Searcy 2001):

$$T_i(t) = \frac{1}{\lambda(t)} \frac{u_i(t)}{\delta_i} [1 - \alpha(t)] \cdot \left[\sigma_i^f + \int_0^t E^c(t-\tau) \frac{\partial \lambda(\tau)}{\partial \tau} d\tau \right] \quad [3.10]$$

where T_i = cohesive zone traction;

u_i = cohesive zone displacement;

δ_i = cohesive zone material length parameter;

$\lambda(t)$ = Euclidean norm of cohesive zone displacements;

$\alpha(t)$ = microscale damage evolution function;

σ_i^f = requisite stress level to initiate cohesive zone;

$E^c(t)$ = stress relaxation modulus of the cohesive zone; and

$i = n$ (opening) or s (shearing).

As presented in Equation [3.10], the cohesive zone damage evolution is characterized by the internal state variable, $\alpha(t)$. It can be noted from Equation [3.10] that when $\alpha(t)$ reaches the value of unity, the crack face traction decays to zero, thus resulting in crack extension. The damage evolution law can be determined by performing fracture tests to represent locally averaged cross-sectional area of damaged material in a cohesive zone. Alternatively, a phenomenological form of the damage evolution can also be employed to represent rate-dependent fracture. In this study, the following simple phenomenological form has been selected, since it is sufficient to evaluate mixtures designed with different aggregate angularities. Parameters *A* and *m* are microscale phenomenological material constants that govern damage evolution behavior.

$$\dot{\alpha} = A[\lambda(t)]^m, \qquad \text{when } \dot{\lambda} > 0 \text{ and } \alpha < 1 \quad [3.11]$$

$$\dot{\alpha} = 0, \qquad \text{when } \dot{\lambda} \le 0 \text{ or } \alpha = 1 \quad [3.12]$$

Cohesive zone elements were embedded within asphalt phase elements and along boundaries between aggregates and asphalt. No cracking was allowed inside the aggregates.

CHAPTER 4
RESULTS AND DISCUSSION

Superpave mix designs of all five mixes were accomplished at UNL. Mix design results are presented in this chapter. Laboratory performance testing results from the uniaxial static creep test, the APA test, and the IDT fracture energy test are then presented and discussed in this chapter. The finite element simulation results of the IDT fracture test are also presented and further discussed in this chapter. Finally, angularity test results estimated from the four coarse aggregate angularity methods and the two fine aggregate angularity testing methods are presented and are further discussed regarding their characteristics to the testing repeatability, cost, testing time, workability, and sensitivity of test results.

4.1. MIX DESIGN RESULTS

Volumetric parameters of each mix are shown in Table 4.1. All mixes were designed at UNL, and representative batches of each mix were sent to NDOR laboratories for validation. As can be seen in the table, no huge discrepancy between NDOR results and UNL results was observed. Mix volumetric properties obtained from UNL laboratory generally satisfied NDOR mix specifications.

Table 4.1. Volumetric Mix Properties

		V_a	*VMA*	*VFA*	P_b (%)	*D/B*
NDOR Specification		4 ± 1	> 14	65 - 75	-	0.7-1.7
CAA = 97	UNL volumetric results	3.8	14.5	73.3	6.0	0.9
FAA = 45.5	NDOR volumetric results	3.6	14.7	75.3	6.0	-
CAA = 90	UNL volumetric results	4.8	14.7	67.6	5.7	1.02
FAA = 45.5	NDOR volumetric results	3.7	14.1	74.1	5.7	-
CAA = 75	UNL volumetric results	5.9	14.3	65	5.4	1.04
FAA = 45.5	NDOR volumetric results	4.5	14.2	68.3	5.4	-
CAA = 90	UNL volumetric results	4.2	14.0	69.8	5.0	0.99
FAA = 43.5	NDOR volumetric results	4.0	13.9	71.3	5.0	-
CAA = 75	UNL volumetric results	4.8	13.9	65.4	4.7	1.05
FAA = 43.5	NDOR volumetric results	4.1	13.7	70.1	4.7	-

4.2. LABORATORY PERFORMANCE TEST RESULTS

4.2.1. Uniaxial static creep test results

Figure 4.1 shows the average flow times obtained from three specimens of each mixture and its standard deviation in the form of an error bar. As shown in the figure, there was an increasing trend in the resistance to rutting as increasingly angular aggregates were placed in the mixtures. This was an expected phenomenon since higher angularity produces better aggregate interlocking. This improved interlocking can increase the rutting resistance of the asphalt mixtures, as has been indicated in other studies (Wedding and Gaynor 1961; Pan et al. 2005; Huang et al. 2009). The contribution of angular aggregates to rutting resistance becomes even more obvious when the binder content of each mixture is considered. As shown in Figure 4.1 by the percentage inside each bar, mixtures with higher binder content were more resistant to rutting, which contradicts a typical observation, namely, that the increase of binder content decreases the rutting resistance. Thus, the effect of angular particles is clearly a factor in the resistance of rutting.

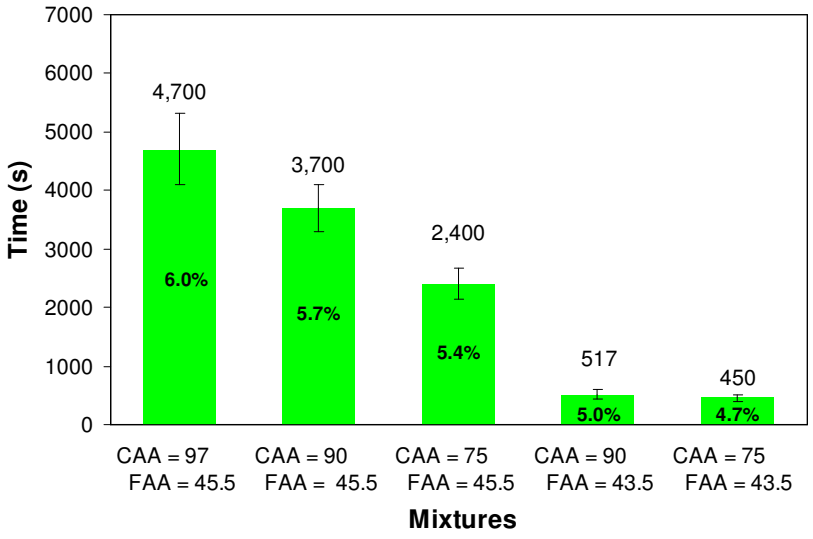

Figure 4.1. Uniaxial Static Creep Test Results

4.2.2. APA test results

Figures 4.2 to 4.5 plot analysis results of APA specimens tested at the NDOR laboratories for the past several years. Instead of using the APA rut depth, a different quantity, rut ratio, was used for the analysis. The rut ratio serves as a replacement for the rut depth and is simply calculated by dividing the total rut depth by the corresponding number of loading cycles and multiplying the obtained value by 100. Rut ratio was employed because the APA test stopped automatically when the wheel loading reached 8,000 cycles before a 12-mm rut depth had been reached or when the total rut depth exceeded 12 mm before 8,000 cycles had passed. Therefore, rut ratio was calculated to provide an equivalent measure of a mixture's rut potential for any case. As can be observed in the figures, APA test results generally present a high testing variability. However, for all mixtures, the simple linear regression implies that the increase of coarse aggregate angularity, which is represented by higher percentage of the number of fractured faces, improved the rutting performance, which supports the results from the static creep test.

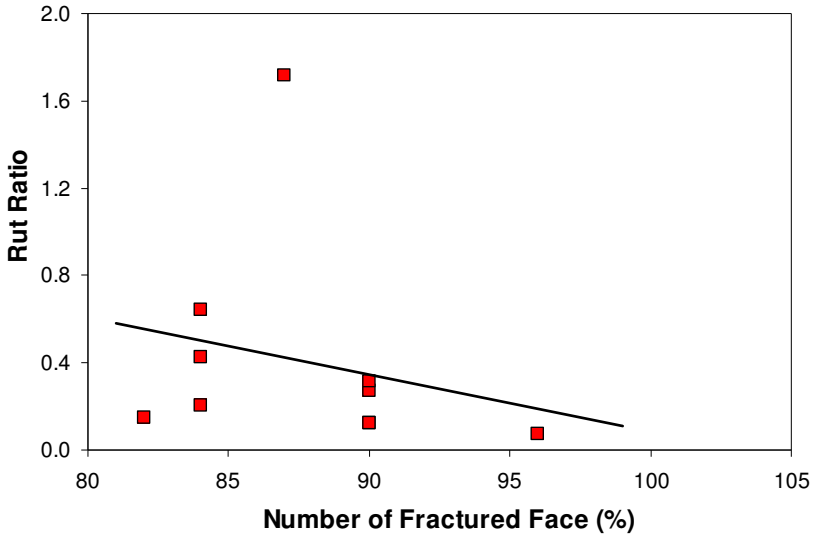

Figure 4.2. APA Test Results of *SP2* Mixtures

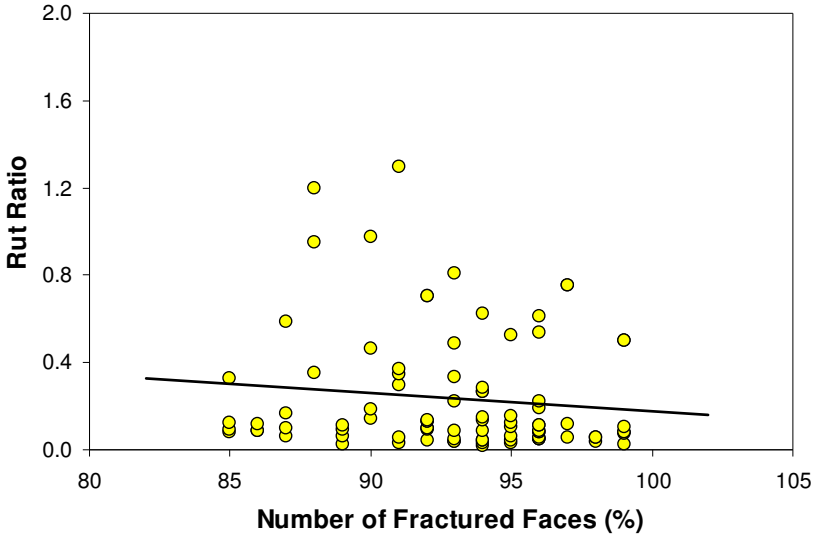

Figure 4.3. APA Test Results of *SP4* Mixtures

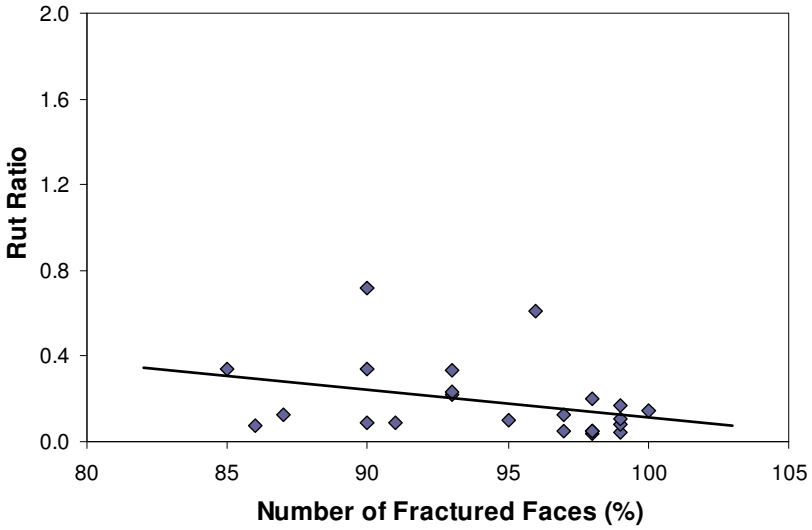

Figure 4.4. APA Test Results of *SP4S* Mixtures

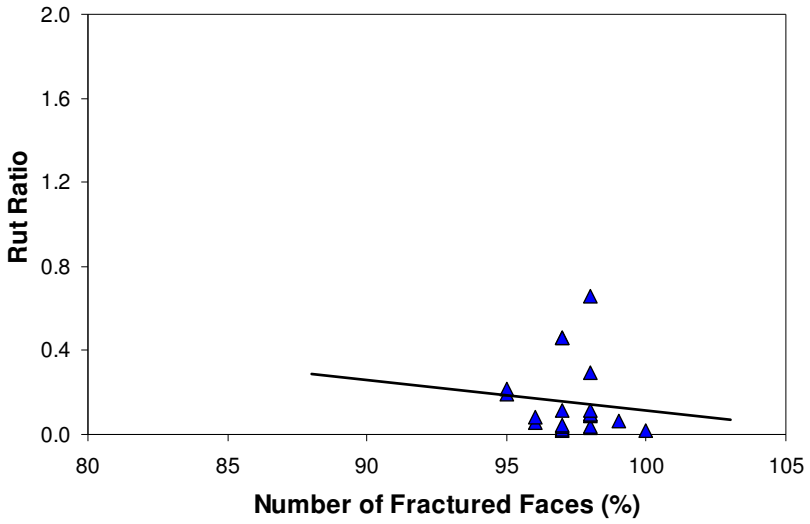

Figure 4.5. APA Test Results of *SP5* Mixtures

4.2.3. IDT fracture energy test results

Figure 4.6 presents test results with average fracture energy and its standard deviation obtained from three specimens of each mixture with the optimum binder content for each mixture shown within each bar. As can be seen in Figure 4.6, mixtures with a higher CAA value produced greater fracture energy, which corresponds to their better resistance to fatigue cracking. In addition, mixtures with different FAA values but the same CAA value showed similar values of fracture energy. As two variables (binder content and aggregate angularity) are involved in the test, both can affect test results. It is generally known that an increase in the binder content of a mixture increases the mixture's fatigue life (Epps 1998) because the binder helps dissipate viscoelastic energy, which results in the stress relaxation of the mixture. On the other hand, the presence of angular particles in the mixture produces a higher stress concentration, which results in the development of more cracks. Thus, from the results of the IDT test for the mixtures with different CAA values but identical FAA values, it can be inferred that the role of the binder might be more significant than the effect of the CAA. This inference agrees with a study by Huang and Grisham (1972) who found that the geometric characteristics of coarse aggregates were not significant in the fatigue behavior of asphalt mixtures. As for FAA,

an examination of the mixtures with identical CAA values but different FAA values in Figure 4.6 shows that the effect of FAA was equivalent but opposite to that of the binder content, which resulted in similar fracture energy between the mixtures.

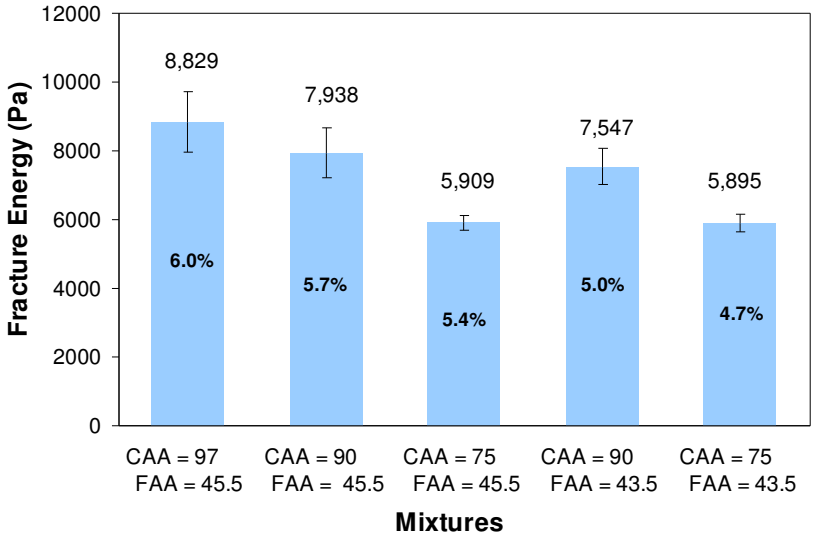

Figure 4.6. IDT Fracture Energy Test Results from Asphalt Concrete Specimens

In order to further investigate the aforementioned inference, the IDT test was performed with fine aggregate matrix mixture specimens to analyze only the effect of angularity. The fine aggregate matrix was produced by mixing aggregate particles of less than 2.36 mm. Two matrix mixtures with different FAA values (43.5% and 45.5%) but with the same amount of binder content were produced for comparison. Since the matrix mixtures were very dense, varying the angularity did not significantly alter the internal volumetric characteristics (such as air voids), even when the same amount of binder (6.0%) was used. Three specimens of each mixture were tested, and test results are presented in Figure 4. Although no dramatic difference between two mixes was observed in the figure, the inference can be supported to a certain extent, as higher angularity increases potential cracking due to stress concentration around the particles.

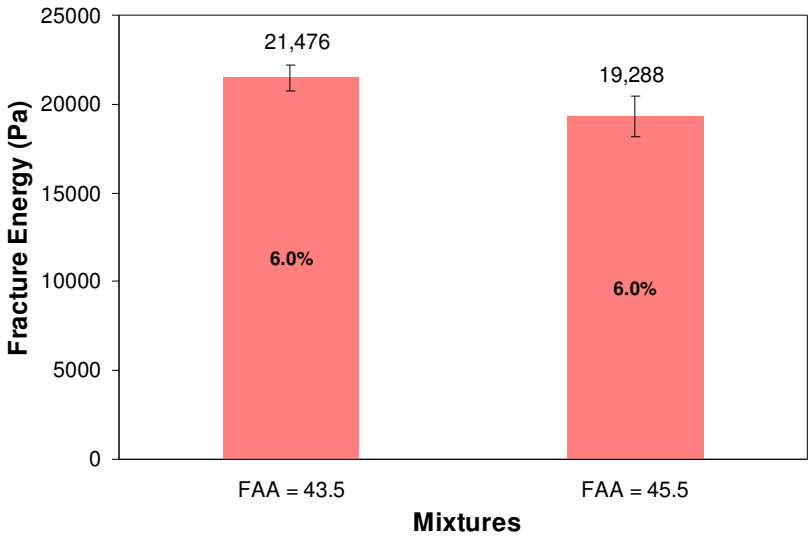

Figure 4.7. IDT Fracture Energy Test Results from Fine Aggregate Matrix Specimens

4.3. FINITE ELEMENT MODEL SIMULATION RESULTS

In an attempt to incorporate the FE simulations with laboratory test results more closely, four virtual IDT specimens were generated, as presented in Figure 4.8. The first specimen (Figure 4.8(a)) was generated with the angularity value of 2,633 (in AIMS), while the second specimen had a target of a higher angularity (2,935). Aside from angularity, all other variables were maintained the same, so that simulation comparisons between two specimens would purely produce the effect of aggregate angularity on cracking behavior. To evaluate the effect of binder content, the third (Figure 4.8(c)) and fourth (Figure 4.8(d)) specimens were generated by varying their aggregate volume fraction with 20% and 15%, respectively, but keeping the angularity constant (2,935 in AIMS) of the second specimen.

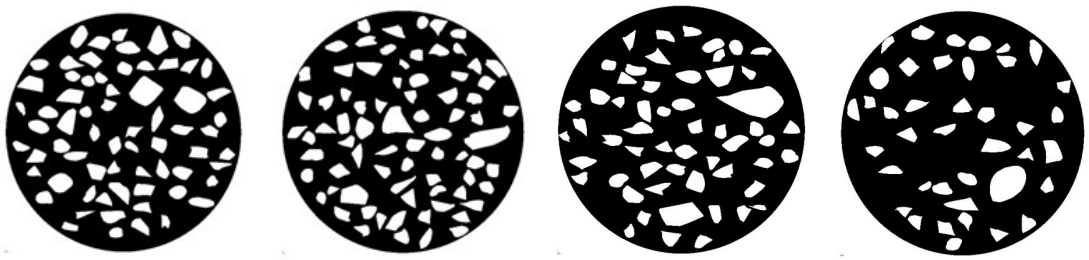

(a) 2,633 and 25% (b) 2,935 and 25% (c) 2,935 and 20% (d) 2,935 and 15%

Figure 4.8. Virtual IDT Specimens Produced for the FE Simulations

For the simulation, the material properties of each phase (aggregates, loading strips, asphalt phase, and cohesive zone) are necessary. As mentioned earlier, aggregates and metal blocks (loading strips) were modeled as linear elastic materials, and the asphalt phase was modeled as a linear viscoelastic material. To simulate cracking and fracture failure, the nonlinear viscoelastic cohesive zone model was used. Material properties of each phase have been reasonably assumed by referring to other studies (Kim et al. 2006a, 2006b, 2007), since the purpose of the simulation for this study was only to capture the qualitative effects of the angularity and volume fraction of the aggregate. Table 4.2 presents linear elastic and linear viscoelastic material properties used for the FE modeling.

Table 4.2. Linear Elastic and Linear Viscoelastic Material Properties

Linear Elastic Material Properties		
Metal Block	E (GPa)	υ
	200	0.29
Aggregate	E (GPa)	υ
	55.2	0.15
Linear Viscoelastic Material Properties		
Prony Series Parameters for Asphalt Phase	Modulus, E_i (MPa)	Relaxation time, ρ_i (sec)
	1.23E+03	0.00003
	2.11E+03	0.0003
	2.00E+03	0.003
	1.26E+03	0.03
	3.45E+02	0.3
	1.13E+02	3
	3.91E+01	30
	1.73E+01	300
	3.51E+01	∞

Several cohesive zone properties are necessary as model inputs to simulate fracture and failure in the IDT testing. The finite element code used herein adaptively inserts cohesive zone elements based on the value of σ_i^f (requisite stress level to initiate cohesive zone). Once the cohesive zone element is included in the object, damage evolution of the cohesive zone is governed by the two material parameters, *A* and *m*, in the damage evolution function, $\alpha(t)$. Cohesive zone failure is then associated with the material length parameter, δ_i which is incorporated with the damage evolution function. Table 4.3 presents cohesive zone model parameters used for this study. Instead of performing any direct fracture tests to obtain parameters, they were reasonably assumed for this study simply to rank-order cracking potential of the four mixtures (shown in Figure 4.8) where their angularity and volume fraction of aggregates varied.

Table 4.3. Cohesive Zone Properties Assumed for This Study

Parameter	Normal Component (*n*)	Shear Component (*s*)
σ^f (MPa)	2.0	15.0
δ (m)	0.01	0.01
A	5.0E+05	5.0E+05
m	2.0	2.0

Simulation results are presented in Figure 4.9 in the form of a bar chart representing fracture energy. The fracture energy of each specimen was calculated from stress-strain curves predicted by the model. As shown in the figure, fracture energy increased as the angularity of the mixture decreased and the asphalt content increased. This is consistent with the IDT test results, as asphalt content positively affects a mixture's fatigue resistance, while angularity lowers resistance to cracking due to sharp corners that cause higher stress concentration.

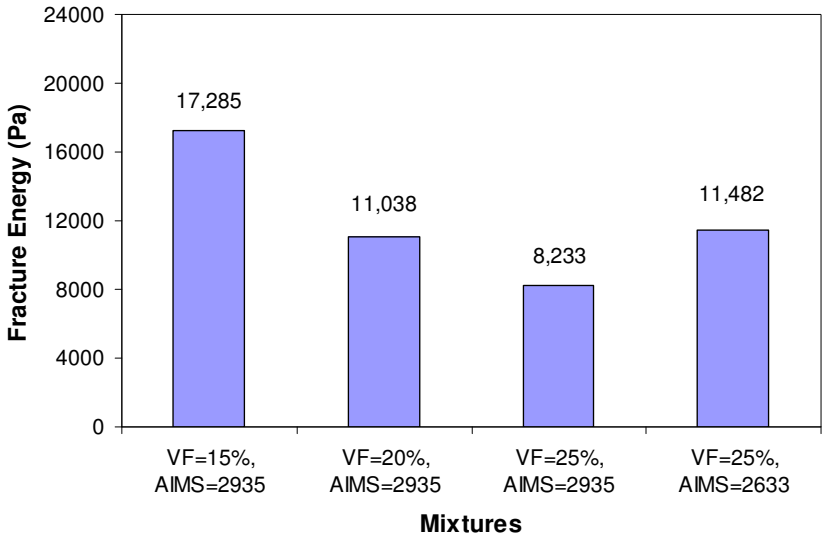

Figure 4.9. Finite Element Simulation Results of the IDT Fracture Energy Test

Figure 4.10 shows the deformation of the specimen (Figure 4.8(b)) and crack growth at two different loading stages (at the peak force and near failure) selected from the force-time curve. Clearly, the deformation of the specimen is increasing due to the accumulated viscoelastic elemental deformation and material cracking. Some cracks develop within the asphalt phase, and others are located at the boundaries between the aggregate and asphalt phases. Further loading after the occurrence of peak force illustrates the development of numerous macrocracks in the specimen, which can be observed by the large decrease in load-bearing capacity.

Along with the result shown in Figure 4.10, the elemental stress contour plots in Figure 4.11 confirm the inferences made from the laboratory IDT test, namely that the sharper corners of the higher angularity aggregates tend to concentrate stresses, thus yielding crack formation and propagation at earlier stages. Figure 4.11 gives a comparison of the stress contour plots between two specimens (Figure 4.8(a) and Figure 4.8(b)) at the same loading level. As can be observed, the specimen with higher angularity presents a higher intensity of stress concentration, which results in lower fracture energy (see Figure 4.9).

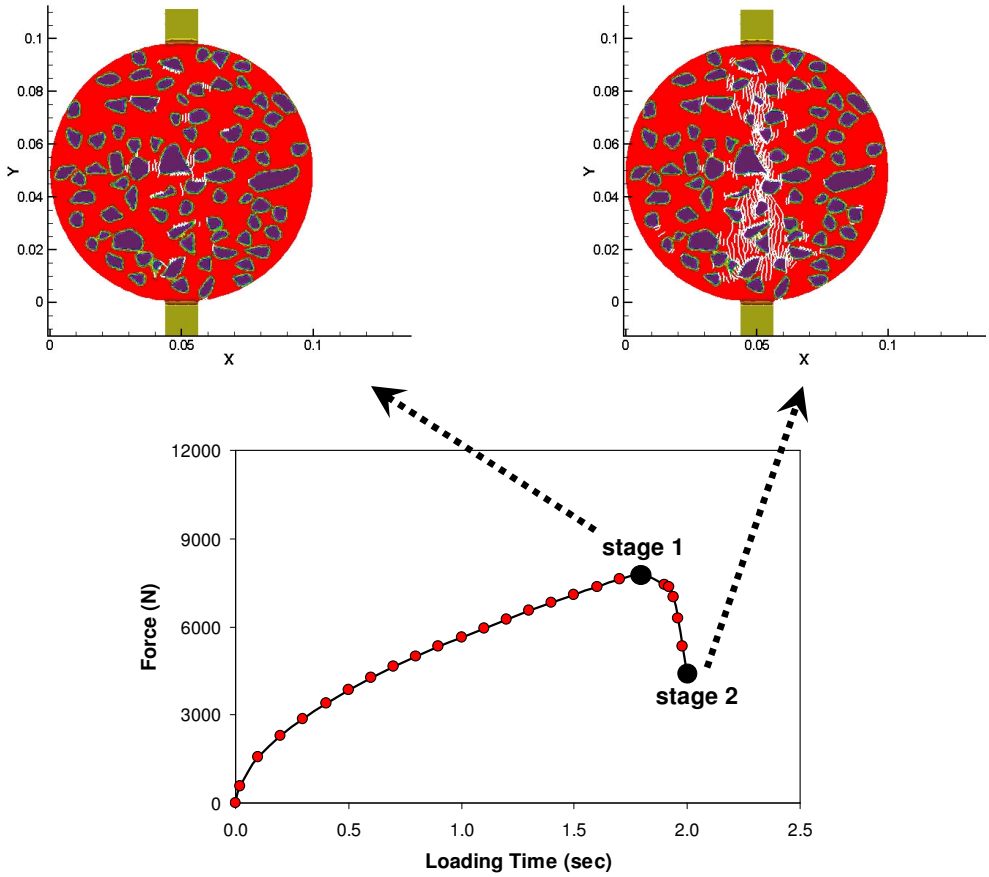

Figure 4.10. Deformation and Crack Growth of the Specimen (Shown in Figure 4.8(b)) at Two Different Loading Stages (at the Peak Force and Near Failure)

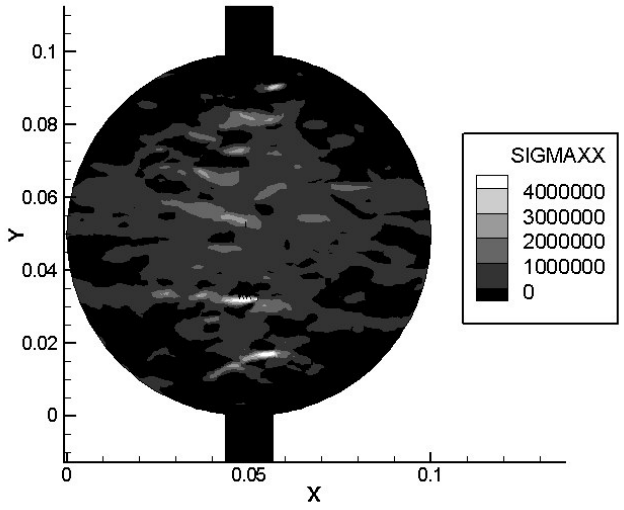

(a) Specimen Shown in Figure 4.8(a)

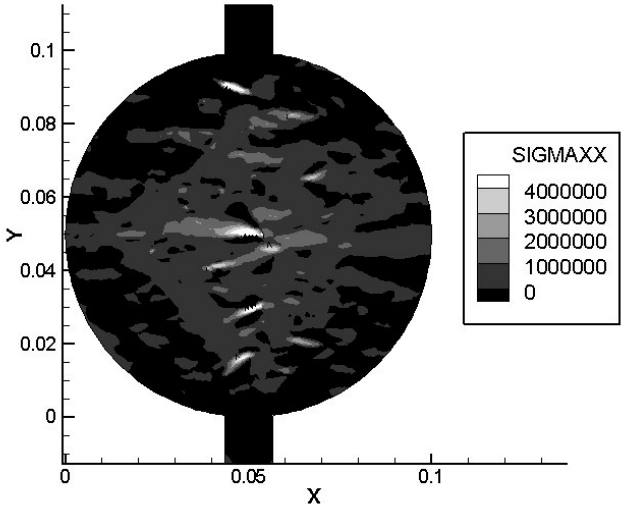

(b) Specimen Shown in Figure 4.8(b)

Figure 4.11. Comparison of Elemental Stress Contour Plots

4.4. ANGULARITY TEST RESULTS AND DISCUSSION

Results from the four different coarse aggregate angularity tests are summarized in Table 4.4. The test results presented for each coarse aggregate (Limestone, 2A, 3ACR-LA, 3ACR-HA, and 47B) are the mean and its standard deviation of three replicates. In order

to achieve more consistent and efficient comparison, the same material was evaluated by the same operator for each different angularity test method. As can be observed in the table, all tests demonstrated an identical trend of angularity values of aggregates: limestone presented the highest angularity value, followed by 3ACR-HA, 3ACR-LA, 47B, and 2A with the lowest value of angularity.

Table 4.4. Summary of Coarse Aggregate Angularity Tests

Angularity Tests	Aggregate Type	Mean	Standard Deviation
ASTM D5821	Limestone	100	0.000
	2A	25.61	1.265
	3ACR LA	90.04	5.000
	3ACR HA	92.85	1.064
	47B	34.98	2.916
AASHTO T326	Limestone	50.23	0.123
	2A	41.98	0.232
	3ACR LA	43.39	0.314
	3ACR HA	46.37	0.521
	47B	42.69	0.113
AIMS	Limestone	2971	27.719
	2A	2051	18.364
	3ACR LA	2240	15.885
	3ACR HA	2484	33.554
	47B	2027	107.968
2-D Digital Image Process and Analysis	Limestone	0.637	0.009
	2A	0.745	0.012
	3ACR LA	0.727	0.001
	3ACR HA	0.707	0.025
	47B	0.731	0.001

Two fine aggregate angularity tests (AASHTO T304 and the AIMS) were performed, and test results are presented in Table 4.5. The test results presented for each fine aggregate are the mean value and its standard deviation of three replicates. Similar to the coarse aggregate angularity analysis, for a better consistency and comparison, the same material was evaluated by the same operator for the two different angularity test methods.

As can be seen in Table 4.5, the two test methods presented a different angularity ranking of aggregates. From the AASHTO T304 method, Screenings presented the highest value (uncompacted void content), followed by 3ACR-HA, 3ACR-LA, 47B, and 2A with the lowest value, whereas, looking at the AIMS test results, 3ACR-HA was the most angular,

following by Screenings, 3ACR-LA, 2A, and 47B with the lowest angularity value. The difference in the two test results can be attributed to the fact that AASHTO T304 measures the uncompacted void content, which is also influenced by other geometric properties such as texture and shape. On the other hand, the AIMS captures only angularity characteristics. Due to the discrepancy, it is recommended that other types of fine aggregate angularity tests be performed with the same aggregates used in this study before making any definite conclusions.

Table 4.5. Summary of Fine Aggregate Angularity Tests

Angularity Test	Aggregate Type	Mean	Standard Deviation
AASHTO T304	Screenings	46.11	0.081
	2A	37.13	0.135
	3ACR LA	43.39	0.166
	3ACR HA	45.27	0.068
	47B	37.51	0.193
AIMS	Screenings	2875.88	18.665
	2A	2329.50	24.923
	3ACR LA	2872.48	21.864
	3ACR HA	3155.30	58.457
	47B	2260.91	39.226

Angularity test results were further analyzed to estimate their characteristics on testing repeatability, cost, testing time, workability, and sensitivity of test results. The definition of each characteristic considered and analysis results are presented here.

Testing repeatability was estimated by the variability of the angularity measurements when one operator repeated the test multiple times using the same material. In order to assess the repeatability, coefficients of variation of measurements were calculated, and resulting values are presented in Table 4.6. As indicated in the table, in the case of coarse aggregate angularity tests, AASHTO T326 (Uncompacted Void Content test) presented the lowest value of coefficient of variation, which implies the highest testing repeatability. ASTM D5821 presented higher testing variability than other test methods. In the case of fine aggregate angularity tests, AASHTO T304 produced more repeatable test results than the AIMS method.

Table 4.6. Repeatability Analysis Results

Aggregate Type	Angularity Test	Standard Deviation	Data Range	Coefficient of Variation
Coarse Aggregates	ASTM D5821	2.049	0-100	3.995
	AASHTO T326	0.261	0-100	0.582
	2-D Image Analysis	0.009	0-1	1.348
	AIMS	40.698	0-10000	1.843
Fine Aggregates	AASHTO T304	0.129	0-100	0.318
	AIMS	32.627	0-10000	1.214

The next category investigated is cost. The cost is defined herein as an estimated price of apparatus and/or testing device required to perform each test. Table 4.7 presents the estimated cost. The cost necessary to perform ASTM D5821 is almost zero, since it simply counts the fractured surfaces of aggregates. To perform AASHTO T326 or T304, a relatively cheap apparatus, which is approximately $500 to $700, is necessary to measure the uncompacted void content in aggregates. For the 2-D digital image process and analysis, a high-resolution scanner and a computer including the image analysis software (ImageTool) are necessary. Compared to other test methods, the AIMS method is the most expensive, because it requires the testing equipment (i.e., AIMS), which is approximately $30,000 to $40,000 in the current market.

Table 4.7. Estimated Price of Each Test Method

Aggregate Type	Angularity Test	Estimated Price ($)
Coarse Aggregates	ASTM D5821	0
	AASHTO T326	500 – 700
	2-D Image Analysis	700 – 1000
	AIMS	30,000 – 40,000
Fine Aggregates	AASHTO T304	500 – 700
	AIMS	30,000 – 40,000

Testing time was then investigated as a parameter to estimate each angularity test. Testing time herein is defined as the approximate time spent to perform the test when the sample is ready. The time spent for the sample preparation was not included in the analysis. Table 4.8 summarizes the time measured for each angularity test. As presented

in the table, the uncompacted void content tests (AASHTO T326 and T304) can be executed much faster than other tests such as ASTM D5821 and the 2-D digital image process-analysis method. The AIMS is also considered a rapid test.

Table 4.8. Testing Time Spent to Perform Each Angularity Test

Aggregate Type	Angularity Test	Approximate Time (min)
Coarse Aggregates	ASTM D5821	40
	AASHTO T326	6
	2-D Image Analysis	60
	AIMS	12
Fine Aggregates	AASHTO T304	6
	AIMS	20

The next category investigated is testing workability. Workability is defined herein as the degree of ease with which a test can be performed, including the handling of the material used, the way the test is performed, and if any special experience is needed to perform the test. Since the testing workability is hard to quantify as a number, narrative descriptions based on the operator's experience are provided here.

In performing the coarse aggregate angularity tests, the ASTM D5821 method is very simple, but must be performed by an operator with experience, otherwise the results are likely very nonrepeatable. The AASHTO T326 test method can be considered easy to perform by any operator, but it requires a large amount of coarse aggregates to perform; also, during the test, it is necessary to strike off excess heaped aggregates from the cylinder by a single pass of the spatula, which may cause different results with different operators. The 2-D digital image process-analysis method is a test that requires an operator with experience in image treatment. Without appropriate experience in image treatment, the enhancement of the image might be performed incorrectly, which will lead to a different result from the original aggregate images. The AIMS approach is the easiest among all test considered, since it is an automated process and is controlled by the software. Therefore, test results are fairly repeatable and are less dependent on testing operators than other methods. In performing the fine aggregate angularity tests, both tests are considered easy to perform, rapid, and generally repeatable. However, similar to the

coarse aggregate case, AASHTO T304 should be performed carefully during the process of striking off excess heaped fine aggregates from the cylinder with the single pass of the spatula.

The last characteristic considered for estimating angularity test methods was sensitivity of testing results. The sensitivity is assessed herein by the ratio of the difference between the angularity values of the most angular and the most rounded materials tested to the whole scale range of each angularity test, as mathematically expressed by the following equation.

$$Sensitivity = \frac{A_H - A_L}{R} \quad [4.1]$$

where A_H = the highest angularity value;

A_L = the lowest angularity value; and

R = scale range of each angularity test.

Table 4.9 presents the sensitivity of each test method. It can be clearly observed that, except for ASTM D5821, testing sensitivity of all methods was very similar, with a value of around 0.1.

Table 4.9. Testing Sensitivity of Each Angularity Test

Aggregate Type	Angularity Test	Angularity Difference	Test Range	Sensitivity
Coarse Aggregates	ASTM D5821	74.39	0-100	0.7439
	AASHTO T326	8.25	0-100	0.0825
	2-D Image Analysis	0.108	0-1	0.1080
	AIMS	920	0-10000	0.0920
Fine Aggregates	AASHTO T304	8.98	0-100	0.0898
	AIMS	894.39	0-10000	0.0894

Based on the analysis results estimating angularity testing characteristics on each category (i.e., repeatability, cost, time, workability, and sensitivity), the ranking of test methods for each category was made and is presented in Tables 4.10 and 4.11.

Table 4.10. Ranking of Coarse Aggregate Angularity Tests for Each Category

Category	ASTM D5821	AASHTO T326	2-D Image Analysis	AIMS
Repeatability	4	1	3	2
Cost	1	2	3	4
Time	4	1	3	2
Workability	4	2	3	1
Sensitivity	1	2	4	3

Table 4.11. Ranking of Fine Aggregate Angularity Tests for Each Category

Category	AASHTO T304	AIMS
Repeatability	1	2
Cost	1	2
Time	1	2
Workability	2	1
Sensitivity	1	1

As summarized in Table 4.10, the AASHTO T326 method is generally ranked higher than other test methods over the several estimation categories considered in this study. In particular, AASHTO T326 seems to perform better than the current Superpave CAA method (i.e., ASTM D5821) in that it is more objective and is very simple to perform with much less testing time. Testing apparatus is not expensive, and the testing quality is not highly influenced by operator's experience. The AIMS approach is also very attractive as a new method that can provide more scientific information of various individual aggregate geometric characteristics separately; however, its relatively high price might be an obstacle for practical implementation.

In the case of fine aggregate angularity test methods, each method demonstrated pros and cons. As shown in Table 4.11, AIMS provides better workability than AASHTO T304, while it requires longer testing time and a much more expensive testing device. The current Superpave FAA testing method, AASHTO T304, seems reasonable in a practical sense, even if the testing result (i.e., uncompacted voids) is not solely the angularity characteristic, but a combined effect of angularity, texture, and form.

CHAPTER 5
SUMMARY AND CONCLUSIONS

A better and more scientific understanding of the effects of aggregate angularity on performance of asphalt mixtures is crucial, given that the angularity requirements for asphalt mix design significantly affect both mix production costs and long-term pavement performance. Thus, this study was conducted to provide guidelines that potentially help improve current Nebraska asphalt specifications, particularly for aggregate angularity requirements and test methods to characterize aggregate angularities based on scientific investigations and experiments. To meet the research objectives, various aggregate angularity tests (four coarse aggregate angularity tests and two fine aggregate angularity tests) were assessed and compared by investigating their characteristics on testing repeatability, cost, testing time, workability, and sensitivity of test results. Then, three laboratory performance tests—the uniaxial static creep test, the APA test, and the indirect tensile fracture energy test—were considered to investigate mixtures' rutting and fatigue cracking resistance from various Superpave mixes designed with different combinations of CAA and FAA values. Results from the indirect tensile fracture energy test were then incorporated with finite element simulations of virtual specimens, which were attempted to explore the detailed mechanisms of cracking related to the aggregate angularity. Simulation results were compared with laboratory test results. Based on the experimental results and numerical simulations, the following conclusions can be drawn:

5.1. CONCLUSIONS

- The AASHTO T326 method generally ranked higher than other CAA test methods considered. In particular, it seems to perform better than the current Superpave CAA method (i.e., ASTM D5821) in that it is more objective and is very simple to perform with much less testing time.

- The current Superpave FAA testing method, AASHTO T304, seems reasonable in a practical sense, although the testing result is not purely angularity characteristic, but a combined effect of angularity, texture, and form.

- The AIMS approach looks very attractive in the sense that it can provide more scientific information of various individual aggregate geometric characteristics separately, but its cost might be an obstacle for practical implementation.

- The analysis of rutting performance showed the same trend in the static creep test and the APA test. That is, increased CAA and FAA in a mixture improved the mixture's resistance to rutting.

- Test results and analyses of fatigue performance data allowed the inference that CAA produces a less significant effect than binder content, while FAA produces an almost equivalent but opposite effect to that of binder content.

- The effect of angularity on fatigue performance could further be evaluated with the test results using fine aggregate matrix mixtures. The increase in FAA was observed to decrease the mixture's resistance to cracking.

- Experimental results were supported by micromechanical finite element simulations. The use of the virtual specimens produced by varying angularities and volumetrics demonstrated clear effects of mixture components and interactions among components on the overall fracture-related mixture performance.

- Model simulations and experimental results indicate that the asphalt binder content positively affects mixture fatigue resistance, while angularity lowers resistance to cracking due to sharp corners, which cause a higher stress concentration.

- Although angular particles develop a higher stress concentration, which can result in cracks, the overall effect of angularity on the mixtures' resistance to fatigue damage

is positive, because aggregate blends with higher angularity typically require more binder to meet mix design criteria. Thicker binder films in the mixture mitigate cracking due to increased viscoelastic energy dissipation from the binder.

5.2. NDOR IMPLEMENTATION PLAN

This research study affirms the necessary balance in design of angularity and binder contents while measuring the effectiveness of current available testing methods. The NDOR will continue to use AASHTO T304 for Fine Aggregate Angularity and ASTM D5821 for Coarse Aggregate Angularity, although AASHTO T326 showed improved CAA test repeatability, the equipment size and sample size is quite cumbersome, and has potential for increased multiple operator variability, due to the requirement to strike off heaping coarse aggregate in a single pass.

The research also confirms that while high angularity is desirable for both FAA and CAA, and higher binder contents help resist fatigue and crack resistance, there is a limit to the improvement that increased FAA's improve the mix and, in research, shows that it will decrease the crack resistance due to stress concentrations at the sharp points of the crushed particles. The research supports the continued direction that the NDOR has been on, and in the past year has been utilizing more designs with FAA's of 43+ and CAA's of 83+, which were first utilized approximately 12 years ago and are exhibiting excellent field performance in various applications. The research also supports and reinforces the NDOR's implementation in the last year of a minimum binder content specification for the current mixes. Equally important in the research were the findings that the modeling and model predictions appear to be quite accurate.

REFERENCES

AASHTO T326, (2005). "Standard Method of Test for Uncompacted Void Content of Coarse Aggregate (As Influenced by Particle Shape, Surface Texture, and Grading)".

AASHTO T304, (2008). "Standard Method of Test for Uncompacted Void Content of Fine Aggregate".

Abbas, A. M. and Shenoy, A. (2005). "Modeling asphalt mastic stiffness using discrete element analysis and micromechanics-based modes." International Jounal of Pavement Engineering, 6(2), pp. 137-146.

Ahlrich, R.C. (1996). "Influence of aggregate properties on performance of heavy-duty hot-mix asphalt pavement." Transportation Research Record 1547, TRB, National Research Council, Washington, DC, pp. 7–14.

Allen, D. H. and Searcy, C. R. (2001). "A micromechanical model for a viscoelastic cohesive zone." International Journal of Fracture, 107, pp. 159-176.

ASTM C1252, (2006). "Standard Test Methods for Uncompacted Void Content of Fine Aggregate (as Influenced by Particle Shape, Surface Texture, and Grading)".

ASTM D3080, (2004). "Standard Test Method for Direct Shear Test of Soils Under Consolidated Drained Conditions".

ASTM D5821, (2006). "Standard Test Method for Determining the Percentage of Fractured Particles in Coarse Aggregate".

Bathina, M., (2005). "Quality analysis of the aggregate imaging system (AIMS) measurements." M.S. Thesis, Texas A&M University, College Station, Texas.

Carlberg, M., C.F. Berthelot, and N. Richardson. (2002). “In-service rut performance of Saskatchewan highways and transportation asphalt concrete mixes.” Canadian Technical Asphalt Proceedings, Calgary, Alberta.

Chowdhury, A., and Button, J. W., (2001). “Fine aggregate angularity: conventional and unconventional approach, aggregate contribution to hot-mix asphalt (HMA) performance”. American Society for Testing and Materials (ASTM) Special Technical Publication, No. 1412, 144–159.

Chowdhury, A., J. Button, V. Kohale, and D. Jahn. (2001). “Evaluation of Superpave fine aggregate angularity specification.” ICAR Research Report No. 201-1, College Station, TX.

Cross, S.A., and E.R. Brown. (1992). “Selection of aggregate properties to minimize rutting of heavy duty pavements.” ASTM STP 1147. American Society for Testing and Materials, Philadelphia, PA, 1992.

Cross, S. A., and Purcell, E. M. (2001). “Effects of fine aggregate angularity on VMA and rutting of Kansas HMA mixtures.” ASTM STP 1412, West Conshohocken, PA.

Dai, Q. and You, Z. (2007). “Micromechanical finite element framework for predicting viscoelastic properties of asphalt mixtures.” Materials and Structures , 41, pp. 1025-1037.

Epps, J. (1998). “Performance of HMA test sections at WesTrack.” Association of the Asphalt Paving Technologists, 67, pp. 738-782.

Foster, C.R. (1970). “Dominant effect of fine aggregate on strength of dense-graded asphalt mixes.” Highway Research Board Special Report 109.

Gonzalez, R. C., and Woods, R. E., (2008). “Digital image processing.” 3rd Edition, New York, Prentice Hall.

Haddock, J., T.D. White, C. Pan, A. Feng, and K. Galal. (1999). "Validation of SHRP asphalt mixture specifications using accelerated testing." Interim Report, National Pooled Fund Study No. 176, West Lafayette, IN.

Hafez, I. (1997). "Development of a simplified asphalt mix stability procedure for use in Superpave volumetric mix design." Ph.D. Dissertation, University of Maryland, College Park, MD.

Hand, A.J., J.A. Epps, and P.E. Sebaaly. (2000). "Precision of ASTM D5821 sandard test method for determining the percentage of fractured particles in coarse aggregate." Journal of Testing and Evaluation, ASTM, Vol. 28, No. 2, pp. 67–75.

Hand, A.J., J.L. Stiady, T.D. White, A.S. Noureldin, and K. Galal. (2001). "Gradation effects on HMA performance." Transportation Research Record 1767, TRB, National Research Council, Washington, DC, pp. 152–157.

Hondros, G. (1959). "The evaluation of Poisson`s ratio and the modulus of materials of a low tensile resistence by Brasilian (indirect tensile) test with particular 67 reference to concrete." Australian J. Appl. Sci., 10(3).

Huang, B., Chen, X., Shu, X., Masad, E., and Mahmoud, E. (2009). "Effects of coarse aggregate angularity and asphalt binder on laboratory-measured permanent deformation properties of HMA." International Journal of Pavement Engineering, 10(1), pp. 19-28.

Huang, E. Y. and Grisham, D. A. (1972). "Effect of geometric characteristics of aggregates on the fatigue response of bituminous paving mixtures." ASTM STP 508, West Conshohocken, PA.

Huber, G.A., J.C. Jones, P.E. Messersmith, and N.M. Jackson. (1998). "Contribution of fine aggregate angularity and particle shape to Superpave mixture performance."

Transportation Research Record 1609, TRB, National Research Council, Washington, DC, pp. 28–35.

Kandhal, P.S., and F. Parker, Jr. (1998). "Aggregate tests related to asphalt concrete performance in pavements.", NCHRP Report 405, Transportation Research Board, National Research Council, Washington, DC, 1998.

Kim, Y.R., J. Daniel, and Wen, H. (2002). "Fatigue performance evaluation of WesTrack asphalt mixtures using viscoelastic continuum damage approach." Final Report No. FHWA/NC/2002-004.

Kim, Y. R. and Wen, H. (2002). "Fracture energy from indirect tension testing." Journal of the Association of the Asphalt Paving Technologists, 71, pp. 779-793.

Kim, Y. R., Allen, D. H., and Seidel, G. D. (2006a). "Damage-induced modeling of elastic-viscoelastic randomly oriented particulate composites." Journal of Engineering Materials and Technology, pp. 18-27.

Kim, Y. R., Allen, D. H., and Little, D. N. (2006b). "Computational model to predict fatigue damage behavior of asphalt mixtures under cyclic loading." Transportation Research Record TRB, 1970, pp. 196-206.

Kim, Y. R., D. H. Allen, and D. N. Little. (2007). "Computational constitutive model for predicting nonlinear viscoelastic damage and fracture failure of asphalt concrete mixtures." International Journal of Geomechanics, pp. 102-110.

Lee, C.J., T.D. White, and T.R. West. (1999). "Effect of fine aggregate angularity on asphalt mixture performance." Final Report, FHWA/INDOT/JTRP-98/20, Purdue University, West Lafayette, IN.

Maerz, N. H., and Lusher, M. (2001). "Measurement of flat and elongation of coarse aggregate using digital image processing." Transportation Research Board Proceedings, 80th Annual Meeting, Washington D.C., Paper No. 01-0177.

Maerz, N. H., and Zhou, W. (2001). "Flat and elongated: advances using digital image analysis." Proceedings of the 9th Annual Symposium of the International Center for Aggregates Research (ICAR), Austin, TX.

Mahmoud, E. M. (2005). "Development of experimental methods for the evaluation of aggregate resistance to polishing, abrasion, and breakage." M.S. Thesis, Texas A&M University, College Station, TX.

Masad, E. A. (2004). "Aggregate imaging system (AIMS): basics and applications." TTI Report 5-1707-01-1, Texas Transportation Institute, College Station, TX.

Masad, E. (2003). "The development of a computer controlled image analysis system for measuring aggregate shape properties." NCHRP-IDEA Program Project Final Report, NCHRP-IDEA Project 77, National Research Council, Washington, DC.

Masad, E., Niranjanan, S., Bahia, H., and Kose, S. (2001). "Modeling and experimental measurements of localized strain distribution in asphalt mixes." Journal of Transportation Engineering, 127(6), pp. 477-485.

Masad, E., Al-Rousan, T., Button, J., Little, D., and Tutumluer, E. (2007). "Test methods for characterizing aggregate shape, texture, and angularity." NCHRP Report 555, Transportation Research Board, National Research Council, Washington, D.C.

Maupin, G.W. (1970). "Effect of particle shape and surface texture on the fatigue behavior of asphalt concrete." Highway Research Record 313.

McGennis, R.B., R.M. Anderson, T.W. Kennedy, and M. Solaimanian. (1994). Background of Superpave asphalt mixture design and analysis. Research Report SA-95-003. FHWA, U.S. DOT.

Mogawer, W.S., and K.D. Stuart. (1992). "Evaluation of test methods used to quantify sand shape and texture." Transportation Research Record 1362, TRB, National Research Council, Washington, DC, pp. 28–37.

Pan, T., Tutumluer, E., and Carpenter, S. H. (2005). "Effect of coarse aggregate morphology on the resilient modulus of hot-mix asphalt." Transportation Research Record, 1929, TRB, pp. 1-9.

Papagiannakis, A. T., Abbas, A., and Masad, E. (2002). "Micromechanical analysis of viscoelastic properties of asphalt concretes." Transportation Research Record, 1789, TRB, pp. 113-120.

Rismantojo, E. (2002). "Permanent deformation and moisture susceptibility related aggregate tests for use in hot-mix asphalt pavements." Doctoral Dissertation, Purdue University, West Lafayette, IN.

Roque, R., B. Birgisson, M. Tia, L. Casanova, and E. Kestory. (2002). "Evaluation of Superpave criteria for VMA and fine aggregate angularity, Final Report, Volume 2: Fine Aggregate Angularity," University of Florida, Gainesville, FL.

Song, S. H., Paulino, G. H., and Buttlar, W. G. (2006). "Simulation of crack propagation in asphalt concrete using an intrinsic cohesive zone model." Journal of Engineering Mechanics, pp. 1215-1223.

Souza, L. T. (2009). "Investigation of aggregate angularity effects on asphalt concrete mixture performance using experimental and virtual asphalt samples." M.S. Thesis, University of Nebraska, Lincoln, NE.

Stakston, A.D., J.J. Bushek, and H.U. Bahia. (2002). “Effect of fine aggregate angularity on compaction and shearing resistance of asphalt mixtures.” Transportation Research Record 1789, TRB, National Research Council, Washington, DC, pp. 14–24.

Stiady, J., Hand, A., and White, T. (2001). “Quantifying contribution of aggregate characteristics to HMA performance using PURWheel laboratory tracking device.” ASTM STP 1412, West Conshohocken, PA.

Stiady, J., K. Galal, S. Noureldin, A. Hand, and T. White. (2001). “Identification of aggregate role in performance of Superpave mixtures employing accelerated testing facility.” ASTM STP 1412, ASTM, West Conshohocken, PA.

Stuart, K.D. and W.S. Mogawer. (1994). “Evaluation of natural sands used in asphalt mixtures.” Transportation Research Record 1436, TRB, National Research Council, Washington, DC, pp. 115–123.

Sukhwani, R., Little, D. N., and Masad, E. (2006). “Sensitivity of HMA performance to aggregate shape measured using conventional and image analysis methods.” TTI Report 0-1707-5, Texas Transportation Institute, College Station, TX.

Tutumluer, E., Rao, C., and Stefanski, J. (2000). “Video image analysis of aggregates.” Final Project Report, FHWA-IL-UI-278,Civil Engineering Studies UILU-ENG-2000-2015, University of Illinois Urbana-Champaign, Urbana, IL.

Wedding, P.A. and Gaynor, R.D. (1961). “The effects of using crushed gravel as the coarse and fine aggregate in dense graded bituminous mixtures.” Association of the Asphalt Paving Technologists, 30.

Weingart, R. L., and Prowell, B. D. (1999). “Specification development using the VDG-40 videograder for shape classification of aggregates.” Proceedings of the 7th Annual

Symposium of the International Center for Aggregate Research (ICAR), University of Texas, Austin, TX.

Wen, H. and Kim, Y. R. (2002). "Simple performance test for fatigue cracking and validation with WesTrack mixtures." Transportation Research Record, 1789, pp. 66-72.

White, T. D., Haddock, J. E., and Rismantojo, E. (2006). "Aggregate tests for hot-mix asphalt mixtures used in pavements." NCHRP Report 557, National Cooperative Highway Research Program. National Research Council, Washington, D.C.

Witczak, M. W., Kaloush, K., Pellinen, T., Basyouny, M. E., and Quintus, H. V. (2002). "Simple performance test for Superpave mix design." NCHRP Report 465, Transportation Research Board, National Research Council, Washington, D.C.

You, Z. and Buttlar, W. G. (2006). "Micromechanical modeling approach to predict compressive dynamic moduli of asphalt mixture using the distinct element method." Transportation Research Record, 1970, TRB, pp. 73-83.

You, Z., Adhikari, S., and Kutay, M. E. (2008). "Dynamic modulus simulation of the asphalt concrete using the X-ray computed tomography images." Materials and Structures, 42, pp. 617-630.

ACKNOWLEDGMENTS

The authors thank the Nebraska Department of Roads (NDOR) for the financial support needed to complete this study. In particular, the authors thank NDOR Technical Advisory Committee (TAC), Moe Jamshidi, Bob Rea, Mick Syslo, Amy Starr, Brandon Varilek, Matt Beran, Lieska Halsey, and Jodi Gibson for their technical support and invaluable discussions/comments. Special thanks go to Dr. Flavio Souza. His wonderful suggestions and critical comments on the finite element model simulations were greatly helpful.